Electrochemically controlled self-assembled monolayers characterized with molecular and sub-molecular resolution

Zhang, Jingdong; Welinder, Anna Christina; Chi, Qijin; Ulstrup, Jens

Published in:
Physical Chemistry Chemical Physics

Link to article, DOI:
10.1039/c0cp02183k

Publication date:
2011

Document Version
Publisher's PDF, also known as Version of record

PCCP

Dynamic Article Links

Cite this: *Phys. Chem. Chem. Phys.*, 2011, **13**, 5526–5545

www.rsc.org/pccp

PERSPECTIVE

Electrochemically controlled self-assembled monolayers characterized with molecular and sub-molecular resolution

Jingdong Zhang,* Anna Christina Welinder, Qijin Chi and Jens Ulstrup

Received 17th October 2010, Accepted 21st December 2010
DOI: 10.1039/c0cp02183k

Self-assembled organization of functional molecules on solid surfaces has developed into a powerful and sophisticated tool for surface chemistry and nanotechnology. A number of reviews on the topic have been available since the mid 1990s. This perspective article aims to focus on recent development in the investigations of electronic structures and assembling dynamics of electrochemically controlled self-assembled monolayers (SAMs) of thiol containing molecules on gold surfaces. A brief introduction is first given and particularly illustrated by a Table summarizing the molecules studied, the surface lattice structures and the experimental operating conditions. This is followed by discussion of two major high-resolution experimental methods, scanning tunnelling microscopy (STM) and single-crystal electrochemistry. In Section 3, we briefly address choice of supporting electrolytes and substrate surfaces, and their effects on the SAM structures. Section 4 constitutes the major body of the article by offering some details of recent studies for the selected cases, including *in situ* monitoring of assembling dynamics, molecular electronic structures, and the key external factors determining the SAM packing. In Section 5, we give examples of what can be offered by theoretical computations for the detailed understanding of the SAM electronic structures revealed by STM images. A brief summary of the current applications of SAMs in wiring metalloproteins, design and fabrication of sensors, and single-molecule electronics is described in Section 6. In the final two sections (7 and 8), we discuss the current status in understanding of electronic structures and properties of SAMs in electrochemical environments and what could be expected for future perspectives.

Department of Chemistry and NanoDTU, Technical University of Denmark, Building 207, Kemitorvet, 2800 Lyngby, Denmark. E-mail: jz@kemi.dtu.dk; Fax: 45 4588 3136; Tel: 45 4525 2352

Jingdong Zhang

Jingdong Zhang, PhD 1996, from Changchun Institute of Applied Chemistry, Chinese Academy of Sciences, supervisor Prof. Erkang Wang. From 1996–1997 she worked as a researcher at Itaya Electrochemiscopy Project (Sendai, Japan) headed by Prof. Kingo Itaya. Since 1998, she has worked in Prof. Jens Ulstrup's group at Department of Chemistry, Technical University of Denmark as a research assistant professor and a research associate professor. In 2009 she joined the faculty as an associate professor in the same department. Her research interests include in situ *scanning tunneling microscopy and electrochemistry of molecular and biological macromolecular monolayers as well as metallic nanostructures.*

Anna Christina Welinder

Anna Christina Welinder obtained her MSc degree in engineering (chemistry) at the Technical University of Denmark (DTU) in 2005. She received a PhD with Prof. J. Ulstrup at DTU in 2010 for studies on insulin adsorption and surface behaviour on monocrystalline Au(111), Au(100) and Au(110) electrode surfaces using STM, AFM and electrochemistry. She was a Carlsberg scholar in 2004 whilst working in J. Ulstrup's group and has won 3 presentation awards. Her research interests include (bio)electrochemistry, charge transport through individual molecules, and surface self-assembled chemistry. She is the author or co-author of 7 research articles and 2 book chapters.

1. Introduction

Organic molecules have been used as additives in metallic electroplating industries for several decades. However, systematic information of molecular adsorption on metallic electrode surfaces at the level of the single atom, ion and molecule first emerged from surface sensitive techniques in ultra-high vacuum (UHV) in the 1980s.[1] For example, application of low-energy electron diffraction (LEED) to determine surface lattices of molecules and anions in the adsorbed state widened immensely our knowledge of surface coverage and molecular orientation at electrochemical electrode surfaces.[1] Such progress was achieved by the introduction of single-crystal electrodes as the substrate surfaces and by the development of surface sensitive techniques with high spatial resolution. In contrast to polycrystalline materials, single-crystal electrodes have precisely determined chemical surface compositions and geometric structures right down to the atomic level, often described as 'well-characterized surface' or 'well-defined surface'.[2] UHV techniques are normally suitable for solid/gas interfaces. However, many species adsorbed on electrode surfaces from solution are sufficiently strongly (*i.e. via* covalent-bonding to the surface) adsorbed so that the surface structures are retained when the sample is transferred from liquid environment to UHV.[3,4] This can explain why some adsorbed organic molecules form similar surface lattices at both solid/gas and solid/liquid interfaces.

One of the most widely studied classes of this kind — in a wealth of different respects — is self-assembled monolayers (SAMs) of alkanethiols at electrochemical and non-electrochemical Au(111) surfaces, in which the unique chemical bonding of Au–S between the gold substrate and the adsorbate and hydrophobic interaction among the chains of neighbouring molecules dominate the molecular packing. A liquid, such as aqueous, environment is here essential for a large number of systems, particularly for hydrogen bonding and other hydrophilic interactions, and for biological systems. Direct mapping of solid/liquid interfaces at the atomic or/and molecular level is therefore highly desirable but also pose tremendous challenges. Scanning probe microscopies (SPMs), especially scanning tunnelling microscopy (STM), invented in the 1980s are surface sensitive techniques with which atomic and molecular resolution also in aqueous electrolyte solution has now been reached. A further attractive merit of the SPMs is that they can be brought to operation in different environments. STM can be carried out in air, in UHV, in a liquid environment, and even in liquid environment under electrochemical potential control. Besides broad applications of SPM in physics, chemistry and biology, SPM has brought a revolution to surface science and even dynamic mapping of surface related processes such as adsorption/desorption, electrochemical reactions and phase transitions at molecular or even atomic resolution has now been achieved.

In the SPM family, STM provides the best resolution so far, though the atomic force microscope (AFM) has also developed rapidly in recent times to approach molecular resolution. The present communication is focused on STM with the aim of studying SAM monolayers at the single-molecule level. The appellation *in situ* has been used differently by physicists and chemists, referring to the solid/gas interface and the solid/liquid interface, respectively. We shall here refer the notion *in situ* STM to the operation of STM in liquid environments and under electrochemical potential control, also often denoted as *in situ* electrochemical STM.[5] We shall use the term UHV-STM for STM used for solid/gas systems in vacuum. Time-dependent dynamics studies of molecular adsorption in liquid environment using STM has also been called *in situ* STM[6–8] which is, however, a special case since the substrate electrode potential was in fact the open circuit potential (OCP). We shall denote this as *in situ* STM without potential control.

Certain organic molecules (or anions) can self-assemble and form ordered two-dimensional monolayers on metallic solid surfaces. The driving forces are either weak (physi-sorption) or

Qijin Chi

Qijin Chi received his PhD degree in analytical and physical chemistry in 1994 from the Changchun Institute of Applied Chemistry, Chinese Academy of Sciences. After one year at Tuebingen University, Germany and two years in Tokyo, Japan, he joined the Department of Chemistry, Technical University of Denmark in 1998. He is currently a lektor (associate professor) in chemistry. Qijin Chi also studied molecular biology and biochemistry (2000–2003) at the Johns Hopkins University School of Medicine. His research interests include nanomaterials, molecular and physical electrochemistry, surface self-assembled chemistry, and biophysical chemistry. He has authored four patents, over sixty peer-reviewed articles and several book chapters.

Jens Ulstrup

Jens Ulstrup graduated in chemistry 1964 and obtained the Dr Scient. degree in 1981, both at University of Copenhagen. Since 1966 affiliated with Technical University of Denmark (DTU), from 1984 as a full professor. Visiting scientist at University of Oxford, The A.N. Frumkin Institute of Electrochemistry of the Russian Academy of Sciences, Fritz-Haber-Institut der Max-Planck-Gesellschaft, and Utah State University. Visiting professor at School of Chemistry, University of Sydney. Member of the Royal Danish Academy of Sciences and Letters and recipient of national and international awards. His present research focus is single-molecule science in charge transport of metalloprotein and DNA-based systems.

strong interactions (chemi-sorption) between the molecules and the electrode surface and intermolecular interactions. The stability of the monolayers depends largely on the interaction between the molecules and the substrate for non-polar molecules but lateral intermolecular interactions and solvation forces contribute almost equally when the molecules are strongly polar or electrostatically charged. SAMs based on chemical Au–S bonds were first reported in 1983[9] and immediately attracted enormous attention. Systematic studies of their surface structures, properties and functions[10–18] have been achieved for a number of molecular systems, driven by a wide range of potential applications.[19,20] Besides Au–S bonding, metallic substrates can also be other transition metals such as silver and platinum.[21] Densely packed, highly ordered SAMs form spontaneously either at solid/gas or solid/liquid interfaces. Both 'dry' methods such as UHV techniques and 'wet' chemical methods such as electrochemistry techniques have therefore been used to characterize SAMs in detail. This offers a unique chance for full understanding of the SAM structure and formation in these two environments. Fig. 1 illustrates SAM formation at a solid/liquid interface from solution. Gold and alkanethiol represent metallic surfaces and thiols with functional groups respectively.

Adsorption/desorption of anions and organic molecules at metallic electrode surfaces affects strongly the electrochemical reactivity of the electrode surface and has long been one of the most central areas in electrochemical sciences.[22–25] Besides a range of pure electrochemical methods such as voltammetry, chronocoulometry and impedance spectroscopy, a number of surface sensitive techniques have been combined with electrochemistry and developed into overall *in situ* techniques. Research on organic molecular adsorption on single-crystal electrode surfaces has been most fruitful. Potential induced phase transitions in different monolayers of organic molecules have, for example been discovered,[26,27] and hydrogen bonding within the monolayers have been found to play a key role in the formation of surface lattices.[28] Surface structures of representative organic molecular monolayers and metal complexes at solid/liquid interfaces mainly based on *in situ* STM in a wide range of recent studies, are summarized in Table 1.

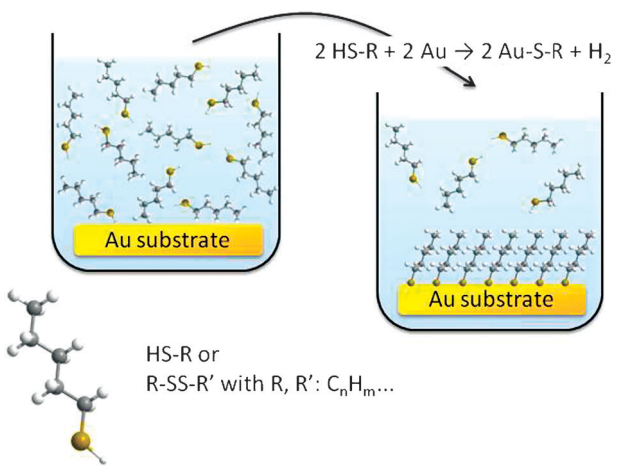

Fig. 1 Schematic illustration of the SAM formation at a solid/liquid interface. Alkanethiol and Au(111) are representatives of a thiol and a metallic surface, respectively. The solution is shown in blue.

Adlayer structures of both thiol[41,42,64,75] and nonthiol containing molecules[29–31,44,50–54,76] have been found to display notable electrochemical potential dependence, suggesting that the electrochemical potential is a key controlling parameter in the monolayer formation. The main objective of the present communication is to illustrate potential dependent SAM structures and formation processes by examples of SAM structures at atomically flat single-crystal gold surfaces in aqueous solution. The focus is on thiol containing molecules. Both hydrophobic and hydrophilic thiols with straight and branched chains, and with positively and negatively charged end groups are chosen. Neutral solutions are preferred with a view on bio-related applications of SAMs. *In situ* STM under electrochemical potential control and single-crystal electrochemistry have been employed as major tools for the investigations of both steady-state electronic structures and surface dynamic processes of the SAMs at the single-molecule level.

2. Experimental methods

2.1 *In situ* scanning tunnelling microscopy

The working principle of STM rests on the quantum mechanical tunnelling effect, as shown in Fig. 2A (left). A tunnelling current flows when a sharp STM tip is scanned over a conductive substrate by applying a bias voltage between the tip and substrate. The tunnelling currents can be converted into topographic images mapping the electronic structures of the substrate. The STM resolution mainly depends on the quality of the tip and substrate and can reveal topographic mapping at the atomic level. Since its invention in the early 1980s, scientists have realised that STM can be brought to operation in multiple environments such as ultra-high vacuum (UHV), air and liquid. The first use of STM investigating solid/liquid interfaces was reported in 1986.[77] *In situ* STM was developed by combining STM with electrochemistry in the late 1980s,[78,79] illustrated schematically in Fig. 2A (middle). Reference and counter electrodes are contained in the STM cell together with electrolyte solution, while the STM tip is insulated except for its outermost end.[78,79] In such configuration, both the STM substrate and tip are fully controlled by the electrochemical potential *versus* a common reference electrode. Using *in situ* STM, reconstruction of metallic electrode surfaces at the solid/liquid interfaces under electrochemical potential control,[80] metal deposition,[81–83] anion adsorption[25,84,85] and organic molecule adsorption[82] have been characterized at atomic or/and molecular level. *In situ* STM has even been employed for nanofabrication of metallic nanoclusters or pits with precise positioning and designed patterns on the well defined surfaces.[86–89]

Environmentally controlled *in situ* STM has recently been developed,[90] as shown in Fig. 2A (right). The motivation for such modifications is to eliminate the influence of dioxygen. It turns out that an anaerobic environment is essential to improve image resolution significantly for many oxygen sensitive molecules such as cysteamine,[74] homocysteine,[75]

Table 1 Surface structures of SAMs for representative organic molecules and metal complexes at solid/liquid interfaces based on *in situ* STM investigations

Molecule	Substrate	Surface structure	Electrolyte	Ref
2,2′-Bipyridine	Au(111)	Phase transition	$NaClO_4$	29 and 30
4,4′-Bipyridine			$KClO_4$	31
4-Mercaptopyridine	Au(111)	$(5 \times \sqrt{3})$	$HClO_4$	32–35
		$(1 \times \sqrt{3})$, $(5 \times \sqrt{3})$, $(10 \times \sqrt{3})$	H_2SO_4	36,37
		$(5 \times \sqrt{3})$	Na_2SO_4	37
Thymine	Au(111)	$c(\sqrt{3} \times 4)$	$HClO_4$ + $KClO_4$	38
		$(2\sqrt{3} \times 2\sqrt{3})$	$HClO_4$	39
Tetramethylthiourea	Au(111)	(3×3)	H_2SO_4	40–42
Thiourea	Au(111)	Short strings	$HClO_4$	43
Trimesic acid	Au(111)	Phase transition	$HClO_4$	44
1,3-Benzenedicarboxylic acid	Au(111)	Ordered monolayer after positive potential annealing	$HClO_4$	45
Benzoic acid	Au(111)	Ordered structure	$HClO_4$	46
1,1′-Binaphthyl-2,2′-dicarboxylic acid	I/Au(111)	Ordered structure	$HClO_4$	47
Metal–porphrin	I/Au(111)	Ordered structure	$HClO_4$	48–49
Metal–porphrin	Au(111)	Ordered structure, potential dependent	$HClO_4$	50–52
Metallophthalocyanine	Au(111), Au(100)	Ordered structure	$HClO_4$	52–54
Fullerene and its derivatives	Au(111)	Ordered structure	$HClO_4$	55 and 56
$[PtCl_6]^{2-}$	Au(111)	$(\sqrt{7} \times \sqrt{7})R19.1^\circ$	$HClO_4$	57
		Disordered	$HClO_4$	58
$[PtCl_4]^{2-}$	Au(111)	$(\sqrt{7} \times \sqrt{7})R19.1^\circ$	$HClO_4$	58
		$(\sqrt{7} \times \sqrt{7})R19.1^\circ$	H_2SO_4	59
	Au(100)	$(3 \times \sqrt{10})$	H_2SO_4	59
$[PdCl_4]^{2-}$	Au(100)	$(3 \times \sqrt{10})$	H_2SO_4	60 and 61
n-Alkanes	Au(111)	Ordered structure	Alkane	62
Ethanethiol	Au(111)	$(p \times \sqrt{3})$, (4×3)	H_2SO_4	63
Short alkanethiols with $-CH_3$ or	Au(111)	Disordered	H_2SO_4	64
$-NH_2$, –OH, –COOH, and –SH end groups	Au(111)	Ordered structure, after reductive desorption	H_2SO_4	64
Benzyl mercaptan	Au(111)	$c(15 \times \sqrt{3})$, $(2 \times \sqrt{3})$	H_2SO_4	65
4-Nitrothiophenol	Au(111)	50% ordered	H_2SO_4	66
Mercaptopropionic acid (MPA)	Au(111)	Strips, $(p \times \sqrt{3})$, p = 5,6,8,10, $(3 \times 4\sqrt{3})$	Phosphate buffer, pH 7	67
		$(p \times \sqrt{3})$, $(3\sqrt{3} \times \sqrt{7})$	H_2SO_4	68
		Cluster, $(2\sqrt{3} \times 5)R30^\circ$	Phosphate buffer, pH 7.9	69
Propanethiol	Au(111)	$(2\sqrt{3} \times 3)R30^\circ$	NH_4Ac (pH 4.6)	70
	Au(100)	Quadratic and a distorted hexagonal structure	H_2SO_4	71
Butanethiol	Au(111)	$(\sqrt{3}\times\sqrt{3})R30^\circ$, $c(4\times2)$	*Ex situ*	6 and 7
		$(2\sqrt{3} \times 3)R30^\circ$	NH_4Ac (pH 4.6)	72
	Au(100)	50% islands + ordered strips	H_2SO_4	73
Cysteamine	Au(111)	$(\sqrt{3} \times 4)R30^\circ$ (O_2-free environment)	NaAc, pH 6.0	74
Homocysteine	Au(111)	$(\sqrt{3} \times 5)R30^\circ$ (O_2-free environment)	Phosphate buffer pH 7.7	75
Oligopyridines	Au(111)	Potential dependent	H_2SO_4	76

and Fe–S proteins such as ferredoxin[69] and heme proteins.[91] A simple example is shown in Fig. 2B. As the smallest ω-functionalized alkanethiol, cysteamine is a short thiol with $-NH_2$ as terminal group. Both amine ($-NH_2$) and thiol (–SH) groups can be partially oxidised in the presence of dioxygen. Argon (Ar) is an inert gas and heavier than air or dioxygen. The presence of Ar in the environment control chamber can reduce the amount of dioxygen in the liquid solution. In the presence of Ar, the bare Au(111) surface is covered by highly ordered $(\sqrt{3} \times 23)R30^\circ$ herring bone structures, which is a typical feature of reconstruction for a clean Au(111) surface. This means that Ar is not adsorbed on the Au(111) surface.[90] Fig. 2B shows representative *in situ* STM images of a cysteamine monolayer on the Au(111) surface in the absence (left) and presence (right) of Ar. Cysteamine molecules form domains with a periodic distance of 11.7 (±0.3) Å between the strips along the direction perpendicular to the atomic rows of the Au(111) substrate. No clear feature could be achieved within each strip by *in situ* STM in ambient atmosphere, Fig. 2B (left). In contrast, Ar-protected *in situ* STM gave clear images of the same monolayers, with stronger tunnelling current signals. Two rows of spots are clearly visible in each strip, Fig. 2B (right). The distance between neighbouring spots along the rows is 5.1 (±0.2) Å, suggestive of $\sqrt{3}$ times a gold atom diameter. A rectangular unit cell, indicated by a blue box, is therefore assigned to a $(\sqrt{3}\times4)$ R30° structure. Each unit cell contains two white spots, which correspond to two cysteamine molecules. High-resolution images further show

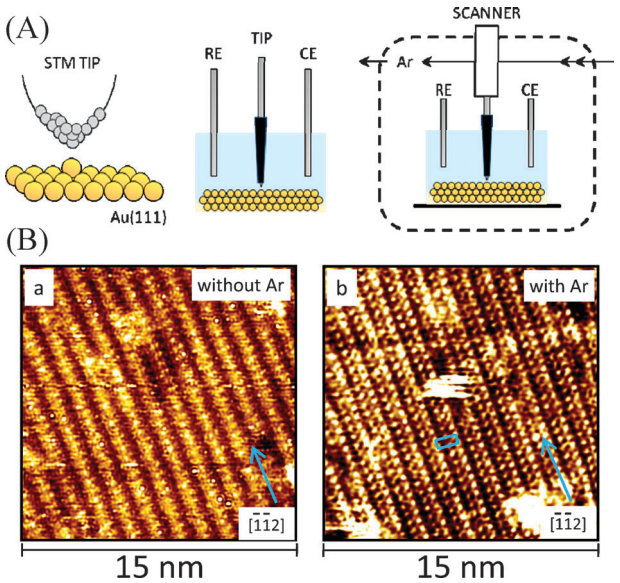

Fig. 2 (A) Schematic drawings of STM (left), *in situ* STM (middle) and environmental gas controlled *in situ* STM (right). RE and CE represent reference electrode and counter electrode, respectively. (B) *in situ* STM images of a cysteamine monolayer on Au(111) in 5 mM NaAc (pH = 6.0). Scan area: 15×15 nm^2. Image obtained without Ar (a) and with Ar protection (b). The blue rectangle in (b) indicates a unit cell containing two cysteamine molecules.[90]

that the two spots in each unit cell have different tunnelling contrast.[74,90]

It is not fully understood why *in situ* STM resolution is affected by O_2, but blurring is significant for many oxygen sensitive systems. The environmental control chamber is efficient enough to remove dioxygen from electrolyte solutions. It is thus expected that the setup (Fig. 2A right) can be further used for investigations of other gas related systems such as CO, CO_2, H_2, and NH_3 at solid/liquid interfaces by *in situ* STM.

2.2 Single-crystal electrochemistry

Pure and applied electrochemistry methods have evolved remarkably over the last few decades,[92] which can almost be likened to a renaissance of the electrochemical sciences. This evolution was prompted, broadly by new and close interaction between electrochemistry and other physical surface sciences. Introduction of single-crystal electrodes, ultrapure chemicals and ultra-clean experimental conditions have, however, been prime movers towards lifting conventional electrochemistry to a higher level dominated by single-crystal electrochemistry. Notably, this evolution has extended to both experimental and theoretical physical electrochemistry and to bioelectrochemistry of biological macromolecules such as redox metalloproteins and DNA-based molecules. The merits of single-crystal electrochemistry are obvious. *First*, well-defined electrode surfaces with a precisely known surface organization of atoms and true geometric area offer both qualitative and quantitative information which can be directly compared with results from other surface sensitive techniques, such as STM, AFM and LEED. A combination of single-crystal electrochemistry with STM can offer complementary information regarding molecular SAM packing and mechanisms of electron tunnelling through molecules. *Secondly*, the signal-to-background ratio is significantly improved and the detection limit notably lowered. *Thirdly*, and along this line, the SAM functionalized surfaces can be constructed and investigated with molecular resolution.[93] The latter two advantages are particularly crucial for obtaining *in situ* STM images and the redox signals of biological macromolecules due to their large geometric size and low coverage on electrode surfaces. Successful examples are represented by comprehensive investigations of metalloprotein monolayers, for example of azurin[94–96] and ferredoxin,[69] both with well controlled molecular orientations at SAM-modified Au(111)-electrode surfaces.

1-Propanethiol SAMs on Au(111) surfaces stand forward as a prime system for comprehensive single-crystal electrochemical and *in situ* STM targeting. Propanethiol is a small straight-chain alkanethiol with a methyl end group. Although hydrophobic, the molecule is soluble in aqueous solution due to its small size, and highly ordered propanethiol SAMs form spontaneously when Au(111)-surfaces are exposed to aqueous propanethiol solutions, Section 3. Fig. 3A shows cyclic voltammograms (CVs) of Au(111) in ammonium acetate (NH_4Ac), pH 4.6 in the absence (dotted line) and presence (solid line) of 1-propanethiol. The clean Au(111) surface is reconstructed into the $(\sqrt{3} \times 23)$R30° herringbone structure, in a wide potential range of −0.5 to + 0.2 V *vs.* SCE. Lifting of the reconstruction gives a characteristic sharp anodic peak at 0.3 V. This is followed by adsorption/desorption of acetate at positive potentials giving rise to broad anodic peaks at 0.4 and 0.6 V and corresponding cathodic peaks at 0.25 V and 0.52 V. The voltammetric peaks caused by lifting of reconstruction of Au(111) surfaces depends on pH and anions in the solution.[25] Self-assembled organization of 1-propanethiol on Au(111) surfaces is driven by formation of a chemical S–Au

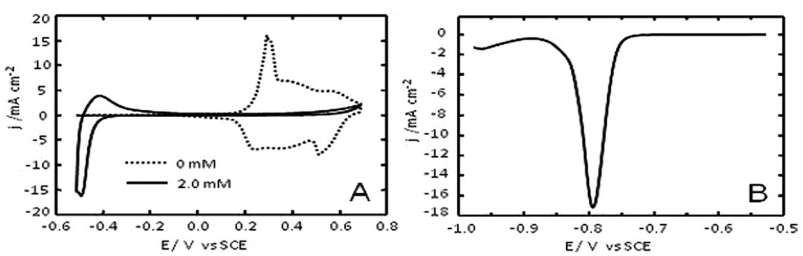

Fig. 3 (A) Cyclic voltammograms of 1-propanethiol covered Au(111) and bare Au(111) in 5 mM NH_4Ac (pH 4.6). The concentration of 1-propanethiol was 0 mM (dotted lines) and 2.0 mM (solid line). Scan rate 50 mV s^{-1}. (B) A linear scan voltammogram for reductive desorption of the propanethiol SAM from the Au(111) surface in 0.5 M NaOH. Scan rate 10 mV s^{-1}.

bond, which is stronger than the adsorption of acetate. The 1-propanethiol SAM can therefore replace the acetate adlayer, resulting in a flat voltammogram in the potential range of 0.0–0.65 V (solid line in Fig. 3 A). A large cathodic current at −0.5 V is due to overlapping of reductive desorption of the 1-propanethiol SAM with dihydrogen evolution. Fig. 3A shows CVs at different two concentrations of 1-propanethiol in solution. The decay of the characteristic acetate adsorption/desorption peak at 0.3 V at a given concentration of thiol reflects formation of SAMs, from which the required concentration of thiol can be found qualitatively.[97] Such information is important for the preparation of SAMs as well as for monitoring the formation process of SAMs by *in situ* STM.

Surface coverage is a key parameter for determination of the population of molecules in the SAMs, which is crucial for interpretation of surface lattices or unit cells. Quantitative values of the coverage can be obtained by voltammetry[98–104] since electrochemical cleavage of the SAM S–Au bonds at negative potential follows reaction eqn (1). This one-electron reductive desorption process[105] should be accomplished in strongly basic solution (pH > 11)[100] to obtain precise coverage values and to avoid interference with dihydrogen evolution as well as to ascertain complete desorption.[106]

$$\mathrm{Au–S–R} + \mathrm{e^-} \rightarrow \mathrm{Au} + \mathrm{^-S–R} \qquad (1)$$

Fig. 3B shows a well-defined sharp cathodic peak at −0.79 V due to reductive desorption of 1-propanethiol SAM from the Au(111) surface in 0.5 M NaOH. The peak potential reflects the strength of the Au–S bond which is determined by the chain length and chemical properties (*e.g.* hydrophobic or hydrophilic) of the terminal groups in the alkanethiol.[101–103] Long-chain alkanethiols with hydrophobic end groups give more negative peaks than shorter alkanethiols with hydrophilic functional groups. The width of the peak reflects the interactions among the molecules in the SAM. Strong interactions such as hydrogen bonds give a narrow peak. In case of 1-propanethiol SAMs at Au(111), the width at half peak height is *ca.* 35 mV (Fig. 3B). This is significantly larger than 15 mV observed for cysteine SAMs[72] but much smaller than 91 mV as expected for a Faradaic single-electron transfer process. These narrow widths testify to the cooperative nature of the reductive desorption process at high-quality single-crystal electrode surfaces.

Reductive desorption of SAMs is a very sensitive probe, from which many factors that affect the Au–S bonding and the local microenvironment can be extracted at least qualitatively. For example, two conformations of the same molecule co-existing in the SAMs result in a detectable splitting of the reductive desorption peak.[74] Appealingly, the Faradaic charge obtained from integration of the reductive desorption peak corresponds to the population of Au–S bonds, *i.e.* the molecular surface coverage in the SAMs. A surface lattice structure obtained from surface sensitive techniques gives a surface coverage of the unit cell, which may include one or more molecules. The surface coverage of molecules as determined by voltammetric reductive desorption helps us to identify features in the unit cell in detail. Surface coverage values of some lattices on Au(111) are summarized in a Table in ref. 72. As an illustration, the surface coverage of 1-propanethiol SAMs on Au(111)-electrode surfaces is found as 7.6 (±0.5) × 10^{-10} mol cm^{-2}, Fig. 3B, which agrees well with those for 1-butanethiol[72] and 1-hexadecanethiol.[102] The unit cell of $(2\sqrt{3}\times3)R30^\circ$ including four spots has been found in high-resolution *in situ* STM images.[70] A comparison of these two sets of data suggests that each spot in the STM images represents a single propanethiol molecule.

The packing patterns of SAMs presented in Section 4.2 have been studied by such combinations of *in situ* STM and single-crystal electrochemistry with an assignment to the level of resolution of the single molecule.

3. Assembly environments

Thiol-containing molecules can be assembled on gold surfaces either from gas phase (“dry” method) or solution (“wet” method). The solvent plays no role in the formation of SAMs in UHV, but has profound effects on the molecular packing of SAMs prepared by “wet” methods. Both the formation dynamics including several intermediate phases and the steady-state SAM structures have been characterized by UHV-STM.[107–111] The advantages of such studies are to offer a fundamental understanding of the formation mechanism as well as the detailed surface structures of the SAMs. However, a broad range of SAMs have been prepared more practically using wet methods. Our focus here is on these SAMs formed from aqueous solutions onto atomically flat gold surfaces. It is, however, also of great interest to compare the *in situ* STM observations with those obtained by UHV-STM.

3.1 Choice of supporting electrolytes

In our present notation, the liquid environment is specified as an aqueous electrolyte solution. STM molecular images in organic solvents have also been reported,[112,113] but aqueous solution is the environment that dominates *in situ* STM investigations as well as the natural environment for biological macromolecules retaining their structure and function. The quality of lab water has now reached a level where the cleanness is in fact comparable with that in an UHV-environment, in the sense that the level of organic and inorganic impurities in the water compares with the residual pressure in UHV-environment. Acids such as H_2SO_4 and $HClO_4$ and their salts are commonly used as supporting electrolytes (see Table 1), while buffers such as acetate and phosphate buffers are recommended electrolytes for neutral pH. Halide ions are often avoided due to their strong adsorption on gold and platinum electrode surfaces. A major concern about the choice of buffer remains, however, as most common buffer molecules, particularly the ones of biological relevance are themselves either strongly adsorbed or even display Faradaic voltammetry on the metallic electrode surface. Many common buffers based on organic molecules thus adsorb strongly on, say gold electrode surfaces giving here huge voltammetric peaks,[114] that make them entirely unsuitable as supporting electrolyte, even though they have been used widely in chemistry and biology in controlling pH of the solutions.

3.2 Type of single-crystal electrode surfaces

Atomically flat surfaces are essential in order to achieve molecular or atomic resolution by *in situ* STM. In general, low-index surfaces are more stable than high-index surfaces. Fig. 4 shows three typical surfaces, *i.e.* bare Au(111), Au(100) and Au(110) observed by *in situ* STM. The ideal geometric atomic surface layer arrangements are shown below each surface. The most characteristic features are the reconstruction lines as assigned to ($\sqrt{3}\times23$)R30°, (5×20), and (1×3) for Au(111), Au(100) and Au(110), respectively. Reconstruction is a common phenomenon for clean metallic surfaces first observed in UHV.[115] ($\sqrt{3}\times23$)R30°, sometimes described as ($\sqrt{3}\times22$)R30° is denoted colloquially as the herringbone structure due to a certain resemblance to a fish backbone structure. Interestingly, the reconstructions of Au(111) and Au(100) give similar patterns in UHV and electrochemical liquid environments.[116] The Au(110) surface is more active. The (1×2) surface structure of Au(110) is the most stable and unique in UHV.[117] In contrast, both the (1×2)[116] and (1×3)[118] structures, as well as mixtures of the two,[119] have been observed by STM in electrochemical environments. The adsorption of anions could be responsible for such differences. The adsorption strength and other adsorption patterns of the same organic molecule are different depending on the surface crystal orientation. This is reflected in the overall SAM structure, an example of which will be discussed in section 4.3.

4. *In situ* STM observations of selected cases

Fig. 5 shows chemical structures of a range of target molecules mapped to single-molecule resolution by *in situ* STM. All these molecules are relatively small and contain a thiol group, but with a variety of terminal groups that determine the chemical properties of SAMs such as hydrophobic and hydrophilic, or electrostatically charged or neutral surfaces. These molecules are sufficiently soluble in aqueous solutions that their SAMs can be prepared and studied in electrochemical environments. Both straight and branched hydrophobic alkyl chains are chosen on purpose with a view on addressing molecular geometric effects on the molecular packing in the SAMs. In addition to the SAM electrostatic charges determined by the end groups such as positively ($-NH_3^+$) and negatively ($-COO^-$) charged groups, the extended hydrogen bond networks among the molecules in the ordered SAMs are key determining factors that strongly affect the lattice structure.

Cysteine, cystine, and homocysteine are highly illustrative in these respects and have been core target molecules in our studies. Cysteine and homocysteine are amino acids. Both are electrostatically neutral molecules in the UHV-environment. The molecular entities are, however, quite different in aqueous solution (pH around 7) where they are converted to zwitter ions with a negatively charged carboxylate and a positively charged ammonium group. The only difference between cysteine and homocysteine is that homocysteine contains one more methylene group in the carbon chain than cysteine. As the dimer of cysteine, cystine holds, further, a disulfide bridge (–S–S–) in addition to two carboxylate groups and two ammonium groups. In the following section, we shall discuss this central *in situ* STM system class in some detail. We shall address both the assembling dynamics in real time and the electrochemical potential dependence of the emerging static structures of the resulting SAMs. Cysteine is a further case where the SAMs of a hydrophilic alkanethiol-based molecule assembled in liquid environment and characterized by *in situ* STM can be compared with similar UHV studies. It appears that cysteine molecules assemble into highly order adlayers specific to the particular crystalline surfaces in both liquid and UHV environments. It seems that the SAM packing in aqueous electrolyte environment depends on the electrolyte composition. Cysteine and cysteine-based target molecules are therefore ideally suited for systematic studies of SAM structures and their dependence on solution pH and on the crystal orientations of the gold substrates.

4.1 *In situ* monitoring of thiol-based assembling dynamics

SAMs consisting of straight-chain alkanethiols on Au(111)-surfaces have attracted most attention due to their high stability and reproducibility. For this reason, 1-propanethiol was chosen as a representative to address assembly dynamics. Formation of SAMs from a liquid environment can be regarded as a dynamic process that depends on the thiol concentration in solution, adsorption time, temperature, and electrochemical potential applied at the substrate. Temperature is known to play an important role towards structural ordering in SAMs for thiols with long chains.[120–123] Temperature is less important for ordered SAM formation of the short-chain

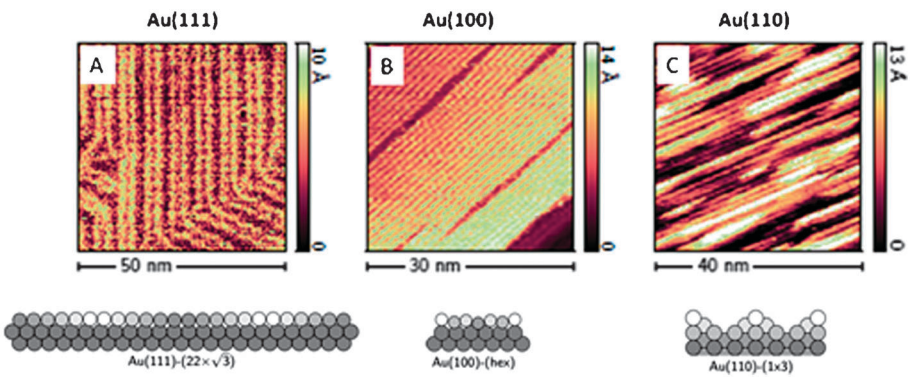

Fig. 4 *in situ* STM images (upper row) of (A) Au(111), (B) Au(100) and (C) Au(110) in 25 mM KH_2PO_4, pH 5. The bottom row shows profile views of the corresponding models.

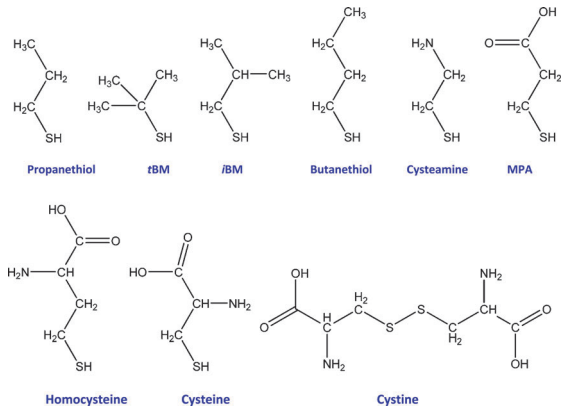

Fig. 5 Chemical structures of some representative thiol-based target molecules.

propanethiol for which highly ordered monolayers are formed rapidly at room temperature. 1.8–2.0 mM 1-propanethiol has been found to be a sufficient concentration for SAM formation as based on electrochemical analysis.[70] It is notable that the dynamic formation process of SAMs has been monitored by *in situ* STM in real time in the whole range from initial molecule injection to full formation of the ordered monolayer, including the electrochemical potential dependence of the process.[70] Fig. 6 A and B show sequential images of the 1-propanethiol SAM formation process at Au(111) surfaces with the difference of large terraces and terrace edges particularly emphasized.

The images shown in Fig. 6A are selected as representatives from a series of images that show in great detail the sequential evolution of the SAM formation process. Fig. 6A:a shows a pattern for a very early stage, in which the reconstruction lines have started to lift at −0.48 V by the presence of 1-propanethiol. ''dark'' patches appear due to *weak electronic contrast*. These patches emerge first in the areas of the *joints* (or ''*elbows*'') between two or three reconstruction lines and give clearly an equilateral triangular shape along the $\{11\bar{2}\}$ directions (*i.e.* $\sqrt{3}$ directions). Corresponding smooth changes were recorded when the substrate potential was shifted slightly positively to −0.45 V, Fig. 6A:b and c. A conspicuous change is an expansion of the area of the dark patches as well as new patches emerging from the elbows, Fig. 6A:e. Some dark patches have started to convert from an equilaterally triangular to an irregular shape, Fig. 6A:d. When the substrate potential was raised to an even slightly more positive value such as −0.41 V, the Au(111)-electrode surface appears to become more active and mobile. As a consequence, many new dark sites rapidly emerge, Fig. 6A:e and f. The formation of dark patches is further accelerated at −0.40 to −0.39 V, and the surface structure changed significantly, Fig. 6A:g and h. The surface microscopic structures are highly sensitive to the substrate potential, even in a narrow range, with significant changes within small positive potential shifts (*e.g.* 10 mV). In addition to new patch sites emerging at the elbows, in Fig. 6A:g and h, the triangular dark patches continue to enlarge along the $\{11\bar{2}\}$ directions. At this stage, the shape of the dark patches becomes more diverse with different shapes co-existing on the surface. Similar dynamic features continue with expansion of dark patches and conversion of equi-lateral triangular to irregular shapes, Fig. 6A:i. A critical potential is reached at −0.38 V. Fig. 6A: j–n, the number of new dark patches is very few, instead with a rapid expansion of already existing dark patches. This feature remains by further shifting the substrate potential positively. The *in situ* observations are focused on time-dependent disappearance of reconstruction lines and formation of pits at this potential. The rapid expansion of the dark patches results in fusion into larger patches, accompanied by disappearance of the reconstruction lines, Fig. 6A:j–n. Meanwhile, pits start to appear on the surface. The initial sites of these pits are preferably located in the boundary regions between the dark patches and the joints of the reconstruction lines. The height of the pits is about 2.4 (±0.2) Å, corresponding to a mono-terrace of Au(111). The population of pits is boosted by the appearance of many small new pits, Fig. 6A:k, l, and new pits emerge along the reconstruction lines depending on their initial locations. Once the reconstruction lines are totally lifted, the number and size of the pits tend to be steady, and the whole surface is covered by SAMs, Fig. 6A:o–p. the pits are mostly in triangle shape following atomic rows of the substrate. 4.0 ± 0.4% of the whole SAM surface area are occupied by pits. In this final stage, the Au(111) surface has been fully covered by a 1-propanethiol monolayer.

The adsorption patterns at the terrace edges and in fact are different from that on the large terraces.[70] Fig. 6B shows a series of images with focus on the edge regions. Fig. 6B:a shows that clean Au(111) terraces with reconstruction lines dominate at the low potential −0.48 V. Smooth terrace edges are found at this potential. When the potential is shifted positively to −0.43 V, corresponding to the same conditions as for Fig. 6A:c, a series of time-dependent changes have been observed, Fig. 6B:b–l. Many small dark patches among the reconstruction lines and some small ripples on the edge of the top terrace start to emerge, Fig. 6B:b. The area of these dark patches increases and some new small patches are formed, Fig. 6B:c. At the same time, shape evolution of the ripples on the terrace edge begins. The ripples first are in a ''zigzag-shape'', and then gradually develop into well defined shapes. Both the area and density of the dark patches increase as expected, while the changes at the terrace edges become even more pronounced, Fig. 6B:d, e. The dark patches fuse together to form larger patches within the terraces, while the terrace edges evolve into tooth-like or saw shape, Fig. 6B:f, g. At this stage, the dark patches are covered by a highly-ordered 1-propanthiol SAM, even though the surface reconstruction was not completely lifted, Fig. 6B:g, h. On the other hand, the saw or tooth-like peninsulae at the terrace edges continue to evolve towards a well-defined triangular shape, Fig. 6B:h. The angle between the 'tooth' sides is 60 ± 5°, and the sides are parallel to the Au(111) atomic row directions. The final stages of the surface evolution are shown in Fig. 6B:j, k. The formation of the SAM close to the terrace edges is completed with a full lift of the reconstruction lines. However, there are much fewer and smaller (only 2–4 nm in diameter) pits in the SAM around the terrace edges, compared to the SAMs on the larger terraces, Fig. 6A. The terrace edge has a saw-tooth-like shape with a sharp fringe, Fig. 6B:i, that finally changes into a smooth fringe, Fig. 6B:k, l.

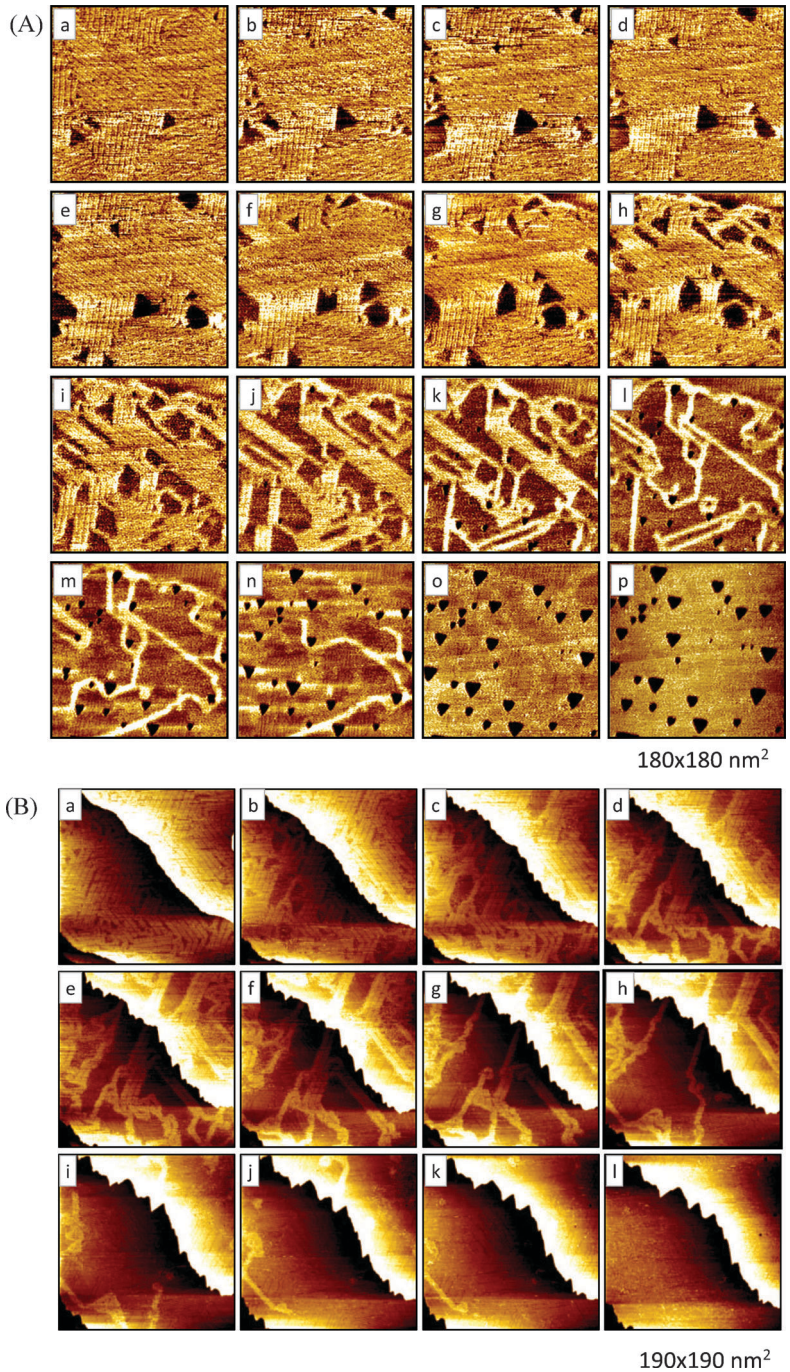

Fig. 6 (A) A sequence of *in situ* STM images for 1-propanethiol SAM formation on Au(111) surface in 1.8 mM propanethiol and 5 mM NH_4Ac (pH 4.6). Focus on large terrace areas. I_t = 0.15 nA, scan area 180 × 180 nm^2. (a) E_w = −0.48 V *vs.* SCE, V_{bias} = 0.13 V, soaking time 3′31″. (b) E_w = −0.45 V *vs.* SCE, V_{bias} = 0.10 V, soaking time 4′55″. (c) E_w = −0.45 V *vs.* SCE, V_{bias} = 0.10 V, soaking time 5′37″. (d) E_w = −0.43 V *vs.* SCE, V_{bias} = 0.08 V, soaking time 6′19″. (e) E_w = −0.41 V *vs.* SCE, V_{bias} = 0.06 V, soaking time 7′01″. (f) E_w = −0.41 V *vs.* SCE, V_{bias} = 0.06 V, soaking time 7′43″. (g) E_w = −0.40 V *vs.* SCE, V_{bias} = 0.05 V, soaking time 8′25″. (h) E_w = −0.39 V *vs.* SCE, V_{bias} = 0.04 V, soaking time 9′07″. (i) E_w = −0.39 V *vs.* SCE, V_{bias} = 0.04 V, soaking time 9′50″. (j) E_w = −0.38 V *vs.* SCE, V_{bias} = 0.03 V, soaking time 10′32″. (k) E_w = −0.38 V *vs.* SCE, V_{bias} = 0.03 V, soaking time 11′14″. (l) E_w = −0.38 V *vs.* SCE, V_{bias} = 0.03 V, soaking time 11′56″. (m) E_w = −0.38 V *vs.* SCE, V_{bias} = 0.03 V, soaking time 12′38″. (n) E_w = −0.38 V *vs.* SCE, V_{bias} = 0.03 V, soaking time 13′20″. (o) E_w = −0.38 V *vs.* SCE, V_{bias} = 0.03 V, soaking time 14′02″. (p) E_w = −0.38 V *vs.* SCE, V_{bias} = 0.03 V, soaking time 14′44″. (B) A sequence of *in situ* STM images of 1-propanethiol SAM formation on Au(111) surface in 1.8 mM 1-propanethiol and 5 mM NH_4Ac (pH 4.6). Focus on terrace edge areas. I_t = 0.15 nA, 190 × 190 nm^2 (a) E_w = −0.48 V *vs.* SCE, V_{bias} = 0.22 V, soaking time: 0′59″. (b)–(l) E_w = −0.43 V *vs.* SCE, V_{bias} = 0.17 V, soaking time: (b) 2′11″, (c) 2′55″, (d) 3′24″, (e) 3′53″, (f) 4′22″, (g) 4′51″, (h) 5′20″, (i) 5′49″, (j) 6′18″, (k) 6′48″, (l) 8′15″.

Under the present experimental conditions 1-propanethiol can be assembled into a highly-ordered monolayer on the Au(111) surface at both the terrace edges and inside terraces, accompanied by lifting of the surface reconstruction. The main differences include: (1) a notable number of triangular pits within the large terraces during thiol assembly, but with no such triangular pit at the terrace edges. Instead, the edges are transformed from a smooth shape into well-defined saw tooth-like fringes. (2) At a given 1-propanethiol concentration, less energy is needed for SAM formation at the terrace edge than within the terrace. The SAM formation at the edge areas can thus be completed at −0.43 V, but at the same potential the reconstruction lines within the terraces are only partially lifted in the same time scale and the SAM formation is far from completed.

Overall, the formation of the 1-propanethiol SAM is accompanied by disappearance of the reconstruction lines, expansion and fusion of the dark patches, and growth of the pits. These events are mutually dependent, which is similar to UHV-STM observations of the alkanethiol SAMs. However, white nano protrusions often found during alkanethiol SAM formation in UHV[109] are not observed by *in situ* STM. This suggests a different formation mechanism in the liquid environment.

In contrast to SAMs of alkanethiols, more complicated formation patterns of SAMs are observed for those thiols with functional groups, in which the influence of the functional groups on dynamic assembling process is significant. For example, several intermediate phases were observed during the formation of cysteamine SAMs on Au(111) surfaces.[74]

4.2 Steady-state structures of representative SAMs

Static structures can be obtained when the development of the SAMs have reached a stable state. High-resolution images show the detailed molecular packing in the SAMs as determined jointly by interactions between the molecules and the substrate as well as lateral intermolecular interactions among molecules in the SAMs. In addition, environmental factors such as solvation are crucial for SAM packing of thiol-based molecules with electrostatically charged end groups. In this section, we focus on the variation of molecular geometric structures, the nature of terminal groups, the surface crystal orientation of substrates, and the solution pH.

4.2.1 Effects of target molecular geometry on the SAM packing. High-resolution *in situ* STM images of three small thiols all with $-CH_3$ end groups but with different straight and branched geometric structures are shown in Fig. 7. All these three thiols form highly ordered structures on the Au(111)-electrode surface. Straight-chain 1-propanethiol forms a $(2\sqrt{3} \times 3)R30^\circ$ SAM lattice (Fig. 7A). Each unit cell contains four spots with different contrasts. Combination with analysis of surface coverage 7.7×10^{-10} mol cm^{-2} from reductive desorption suggests that each spot represents a single 1-propanethiol molecule.[70] This surface structure is close to $(\sqrt{3} \times \sqrt{3})R30^\circ$, frequently reported for straight chain alkanethiols on Au(111) in UHV where, however, the different contrasts of the spots are mostly ignored.[12] The butanethiol SAMs give a similar packing pattern on Au(111),[72] serving together with 1-propanethiol as a reference structure.

Totally different lattices are observed for the two isomers, 2-methyl-1-propanethiol (iBT)[124] and 2,2′-dimethyl-1-propanethiol (*tert*-butanethiol, tBT).[125] Fig. 7B and C show images of SAMs of iBT and tBT, respectively. Strip features appear in the iBT SAMs with a surface structure of $(\sqrt{3} \times 8)R30^\circ$ and a coverage of 5.76×10^{-10} mol cm^{-2}. The surface coverage is smaller than for straight chain alkanethiols (*i.e.* 7.7×10^{-10} mol cm^{-2}). Four iBT molecules are accommodated in each unit cell and intermolecular lateral interactions are strong. In contrast, the uniform $(\sqrt{7} \times \sqrt{7})R19^\circ$ structure corresponding to the low coverage of 3.3×10^{-10} mol cm^{-2} for the tBT SAMs suggests that the lateral intermolecular interaction among the molecules is weak. Such a surface organization and a low surface coverage are caused by the spatially demanding 3-dimensional branched structure of the tBT molecule with three individual methyl end groups.[126] Although hydrophobic interaction dominates among the molecules in all the three SAMs, notable differences among the SAM packing structures of the isomers of three small thiol molecules thus emerge, caused by the geometric differences between the molecular structures.

4.2.2 Effects of terminal groups in target molecules

Packing, intermolecular interactions, and solvation effects are entirely different in thiol-based molecules with hydrophilic polar or electrostatically charged end groups. Such primary groups would be $-NH_2$ and –COOH which are further

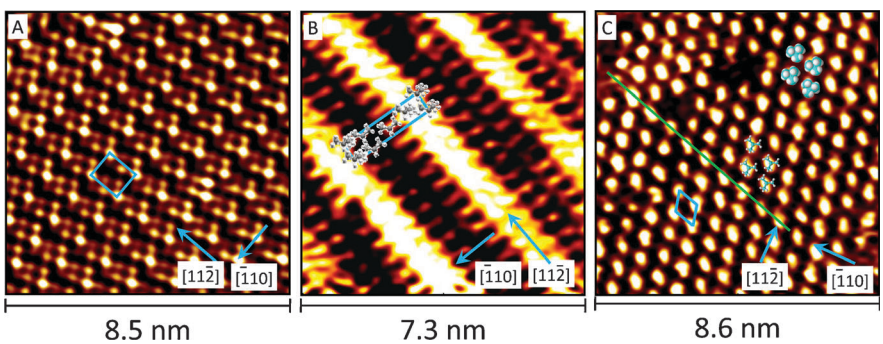

Fig. 7 A comparison of *in situ* STM images of (A) 1-propanethiol,[70] (B) 2-methyl-1-propanethiol (iBT)[124] and 2,2′-dimethyl-1-propanethiol (*tert*-butanethiol, tBT)[125] on Au(111) in NH_4Ac (pH 4.6). Unit cells are marked in blue boxes.

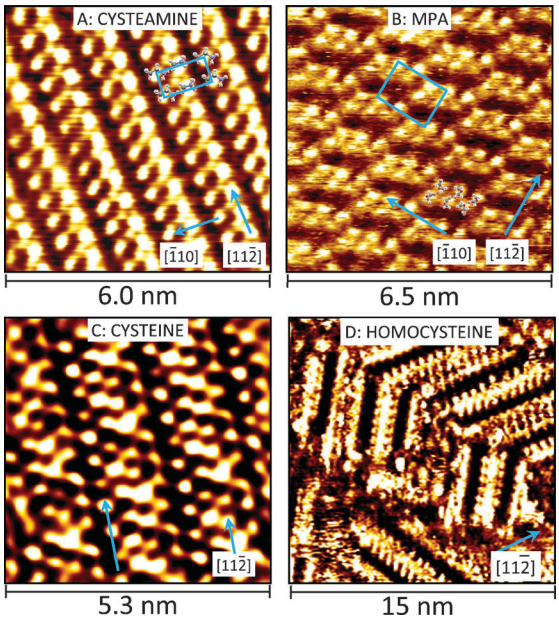

Fig. 8 A comparison of *in situ* STM images of (A) cysteamine,[74] (B) MPA,[69] (C) cysteine[72,129] and (D) homocysteine[75] on Au(111) surfaces in different aqueous buffers.

protonated and deprotonated, respectively in aqueous neutral solution to form positively charged $-NH_3^+$ and negatively charged $-COO^-$. The emerging multifarious packing modes are strikingly illustrated by the SAMs of cysteamine, mercaptopropionic acid (MPA), cysteine, and homocysteine compared in Fig. 8.

The structure of the cysteamine molecule resembles that of 1-propanethiol, with $-NH_2$ instead of $-CH_3$ as the end group. The cysteamine SAMs give a surface coverage of 5.7×10^{-10} mol cm^{-2}, significantly lower than the value 7.7×10^{-10} mol cm^{-2} for 1-propanethiol SAMs. The STM image in Fig. 8A shows a highly ordered adlayer with a $(\sqrt{3} \times 4)$R30° unit cell that has two spots with two different contrasts. A comprehensive analysis based on electrochemical and *in situ* STM experiments and supported by both molecular dynamics and density functional computations indicates that each unit cell includes in fact both *trans* and *gauche* conformations of cysteamine molecules.[74] The different contrasts found in the *in situ* STM images are caused by different tunneling routes through the molecule in the monolayer. This is in turn rooted in different orientations of the two molecules in the unit cell, *i.e.* upright and tilted, for which hydrogen bonding is a main driving force.

MPA SAMs have been investigated by a number of groups using *in situ* STM.[67–69] Several surface lattices have been reported in acid as well as in neutral solutions.[67–69] Fig. 8B shows a STM image of the MPA monolayer in phosphate buffer pH 7.9.[69] In contrast to cysteamine or 1-propanethiol, a large number of clusters form arrays of $(2\sqrt{3} \times 5)$R30° over the whole MPA SAM. Each cluster in the *in situ* STM image is seen to be composed of six spots with the same contrast, corresponding to six MPA molecules, organized in two rows. A plausible reason for the cluster formation is hydrogen bonding among the $-COO^-$ groups within a row as well as between the two rows, mediated by protons or water molecules.

L-Cysteine and cystine (the dimer of cysteine) also form network-like cluster structures in the SAMs.[72] L-Cysteine is the only natural amino acid, which contains a free –SH group in addition to the $-NH_2$ and –COOH groups. Compared with MPA, cysteine has an $-NH_2$ group anchored on the second carbon atom of the molecular chain. A large cluster with $(3\sqrt{3} \times 6)$R30° lattice structure has been found in the monolayer of L-cysteine in acetate buffer (pH 4.6). Similar to the MPA SAMs, six cysteine molecules are organized into two rows in each cluster, Fig. 8C. The differences between MPA and cysteine clusters are the larger size of the cluster and the stronger hydrogen bonding for the cysteine cluster. In comparison, homocysteine does not form a cluster structure, though its structure resembles that of cysteine. Besides the same –COOH and $-NH_2$ groups, the only difference between cysteine and homocysteine is that homocysteine contains one more methylene group than cysteine. Such a structural difference is enough to cause a drastic difference in the SAM packing. A typical *in situ* STM image, Fig. 8D, shows that *ca.* 90% of the Au(111)-electrode surface has been covered by small domains, in which small "saw-tooth" like structures are seen to stack together into a strip feature.[75] The periodic distances in the strips fit well with a $(\sqrt{3} \times 5)$ R30° lattice. The molecular coverage 6.1 ($\pm$0.2) $\times 10^{-10}$ mol cm^{-2} obtained from reductive desorption suggests that each unit cell holds three homocysteine molecules. The 'saw-tooth' features come from hydrogen bonding in the monolayer. Intriguingly, the highly ordered structure is strongly potential dependent, in contrast to many SAMs of other non-redox thiols, such as MPA and cysteine. Homocysteine SAMs give a pair of sharp voltammetric non-Faradaic peaks in the potential range of 0.0–0.05 V *vs.* SCE, and a nicely ordered monolayer appears only at potentials around the sharp peaks. The potential dependent surface changes and the origin of the phenomenon will be discussed in Section 4.5. Presently we note that the additional methylene link in the homocysteine molecule serves

Table 2 Surface structures of cysteine and cystine SAMs in liquids and UHV

Molecule	Substrate	Surface structure	Environment	Ref
L-Cysteine	Au(111)	Quadratic lattice	UHV	130
L-Cysteine	Au(111)	$(\sqrt{3}\times\sqrt{3})$R30°	$HClO_4$	127
		$(4\times\sqrt{7})$R19°	$HClO_4$	128
		$(3\sqrt{3}\times6)$R30°	NH_4Ac, pH 4.6	72 and 129
Cystine	Au(111)	$(3\sqrt{3}\times6)$R30°	NH_4Ac, pH 4.6	72
Cysteine	Au(110)	Cluster	UHV	131
Cysteine	Au(110)	$c(2 \times 2)$	NH_4Ac, pH 4.6 and 6.5	118

as a joint so that both the $-COO^-$ and $-HN_3^+$ groups can bend toward to the substrate surface or fit the formation of hydrogen bonds.[75]

4.2.3 Thiol and disulfide groups: cysteine and cystine/ Au(111) give the same surface structure. As an important amino acid and the only –SH containing natural amino acid, assembling of cysteine monolayers on various substrates in different environments[72,118,127–132] has attracted significant attention ever since their introduction. A variety of L-cysteine and cystine assembling conditions will be addressed in Sections 4.3 and 4.4. As a prelude to this discussion, the surface structures or lattices of cysteine SAMs obtained by UHV-STM and *in situ* STM from different research groups are summarized in Table 2.

Cystine dimer includes a disulfide bridge –S–S– rather than the –SH group as in cysteine. The molecular structure of cystine is shown in the bottom row, Fig. 5. The disulfide bridge in cystine is expected to break and single S–Au bonds to form as the SAMs on the gold surface.[72]

Fig. 9 shows *in situ* STM images of the SAMs of cysteine and cystine on Au(111) in ammonium acetate pH 4.6. Highly ordered clusters are obtained for both SAMs with the same unit cell $(3\sqrt{3} \times 6)R30^\circ$. The clusters show the same size including six cysteine and three cystine molecules, respectively. Reductive desorption peaks from cysteine and cystine are furthermore virtually identical, which means that the peaks appear at the same potential and with the same coverage and half peak width.[72] This indicates that the SAMs of cysteine and cystine are indistinguishable. The only difference is reflected by the critical concentration required for SAM formation. 1 μM and 2.5–10 μM are needed for SAM formation of cysteine[72] and cystine[97] respectively. Cystine dimer thus needs 2.5–10 times higher concentration than cysteine, suggesting that breaking of the disulfide bridge in cystine is a slow process compared with the formation of cysteine SAMs.[97]

4.3 Effects of the substrate crystal orientation

The molecular SAM organization for a given molecule is determined by the interaction with substrate as well as by the environment. The dependence is strikingly illustrated by the organization of the same or similar type alkanethiol-based molecule on different low-index Au-electrode surfaces. A quadratic lattice has, for example been reported for alkanethiol SAMs on Au(100),[71] reflecting the quadratic arrangement of the gold atoms underneath. The cysteine SAMs have been studied in particular detail on Au(111) and Au(110) in both aqueous solution and UHV, as summarized in Table 2. This molecule serves as an example to illustrate the notable effects of the environment and the atomic Au-substrate structures on the SAM structures.

Fig. 10 compares the *in situ* STM images of the cysteine SAMs on Au(111) and Au(110) surfaces in ammonium acetate pH 4.6. Highly ordered lattices are present on both substrate surfaces. The $(\sqrt{3} \times 22)R30^\circ$ reconstruction on Au(111) and the (1×3) reconstruction on Au(110) are lifted in the presence of cysteine. This is in contrast to the observations in UHV, where both cysteine adlayer and herringbone reconstruction lines from Au(111) are visible by UHV-STM.[130,131] Cluster structures are found on Au(111) in both UHV[130] and liquid environment[72] but the unit cell and the cluster size are different, with six and four cysteine molecules assigned to each SAM cluster in liquid and UHV, respectively. This is in contrast to cysteine SAMs on Au(110). No cluster structure is found in the liquid environment,[118] while clusters with eight cysteine molecules are observed by UHV-STM.[132] Both solvation and crystal orientation of the substrate undoubtedly play important roles in controlling the molecular arrangement in the SAMs. Fig. 10 B shows a $c(2 \times 2)$ lattice of L-cysteine monolayers on Au(110). Combined with voltammetric surface coverage analysis each unit cell is found to contain two molecules, each molecule giving three spots in the *in situ* STM image.[118] *Sub*molecular *in situ* STM resolution has thus been reached in this case. Computational support has further led to the assignment of each spot to a particular chemical group, such as –COOH, $-NH_2$ or –SH, *i.e.* to really detailed image interpretation and understanding of the origin of the STM contrasts. No clue as to the interaction among the cysteine molecules in the SAMs has, however, been found in this case.

4.4 Effects of solution pH

pH is well known as a crucial parameter for controlling both the chemical identity of molecular solute species, and the rate and yield of chemical reactions in aqueous solution. With reservations as to molecular identity on transfer from freely solute to the adsorbed state at a solid surface, pH can also be expected to affect the packing in the SAMs for hydrophilic and protic molecules. pH has only little effect on most alkanethiols since the methyl group is inert and stable over a

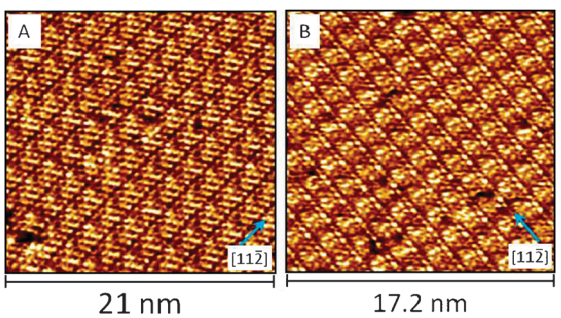

Fig. 9 *In situ* STM images of (A) L-cysteine (monomer) and (B) L-cystine (dimer)[72] on Au(111) in 50 mM NH_4Ac, pH 4.6.

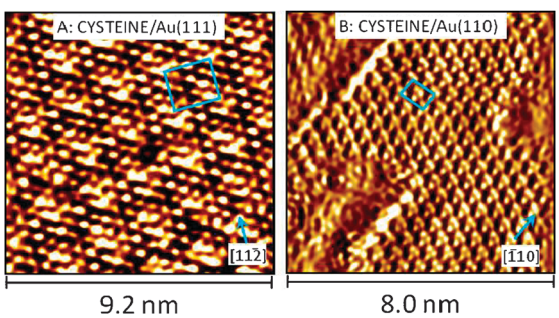

Fig. 10 *In situ* STM images of L-cysteine on (A) Au(111) [129] and (B) Au(110)[118] in NH_4Ac (pH 4.6).

wide pH-range. For this reason, acidic media such as H_2SO_4 and $HClO_4$ are broadly used for *in situ* studies of molecular assembling, as shown in Table 1. For other hydrophilic or protic molecules such as mercapto-carboxylic acids, (MPA), various lattices ($p \times \sqrt{3}$), ($3\sqrt{3} \times \sqrt{7}$), cluster ($2\sqrt{3} \times 5$)R30° and strip features have been discovered in acidic solutions and at neutral pH, respectively.[67–69] Another example is L-cysteine monolayers. Two drastically different surface structures ($\sqrt{3} \times \sqrt{3}$)R30° and ($4 \times \sqrt{7}$)R19° on Au(111) have been reported in $HClO_4$ while a cluster structure of ($3\sqrt{3} \times 6$)R30° is found in NH_4Ac, pH 4.6, *cf.* above. Protonation equilibria of L-cysteine involving the carboxylate group may be a reason for the different lattices observed for SAMs in acidic solutions.

The pH effect is also clearly illustrated by the behaviour of L-cysteine monolayers on Au(110) in neutral and weakly acid solution.[118] A highly ordered $c(2 \times 2)$ structure with two cysteine molecules in each unit cell appears in the SAMs on Au(110) at both pH 4.6 and 6.5, as shown in Fig. 11, suggesting that the $c(2 \times 2)$ lattice is stable in this pH range. Each cysteine molecule gives three *in situ* STM spots organized in a triangular mode, corresponding to thiol, ammonium and carboxylate groups, respectively. The STM contrast of the spots is rather uniform at pH 4.6 (Fig. 11B), but one brighter spot and two weak spots emerge at pH 6.5 (Fig. 11D). Such a contrast change is caused by molecular protonation or deprotonation as SAM dissociation or hydrolysis is not expected to happen under the experimental conditions used. Neither the thiol nor the carboxylate group are likely to be engaged in protonation equilibria in this pH-range, leaving the ammonium group as the most likely candidate. The strong contrast spot in the triangular STM images would then represent the amino group in the cysteine monolayer. This conclusion may, however, well need modification if the Au-surface affects significantly the pK_a-values of the functional

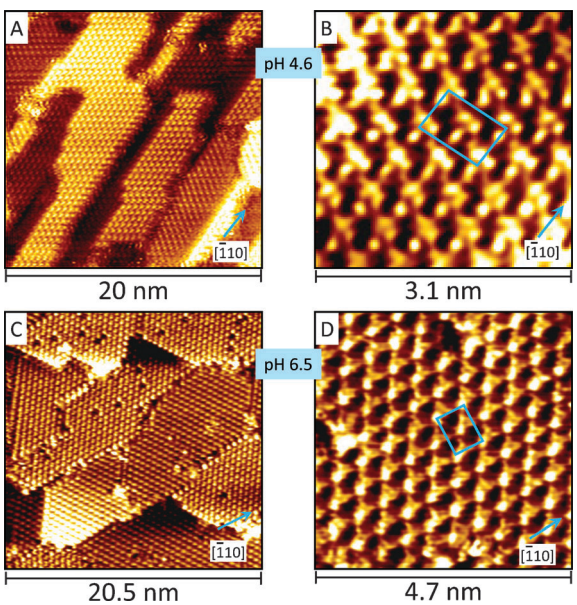

Fig. 11 Solution pH effects on the structures of cysteine monolayers on Au(110) surfaces observed by *in situ* STM.[118] 20 mM NH_4Ac. (A) and (B) pH 4.6, (C) and (D) pH 6.5. Unit cells are marked by blue boxes.

groups. Theoretical approaches offer other detailed understanding of the origin of the STM contrast and will be discussed below (Section 5).

4.5 Effects of the substrate working potential

The substrate electrochemical potential reflects the electronic state of the substrate which, as noted is an important parameter for monolayer assembling as well as for the stability of the SAMs. This parameter can easily be controlled or measured by electrochemical instrumentation. In fact, all the Au–S based SAMs are only stable in a certain potential range. Reductive desorption occurs at negative potentials, oxidative desorption or other Faradaic processes at more positive potentials. The open circuit potential is normally far away from the redox desorption potentials for many long-chain SAMs. In this section we discuss two examples *i.e.* cysteamine and homocysteine, in which the electrochemical potential of the gold substrate plays a key role in the control of the surface structures.

The high structural resolution of cysteamine monolayers in neutral solution including the crucial need for an anaerobic *in situ* STM environment has been discussed in Section 4.2.2. Cyclic voltammetry of the cysteamine monolayer shows two sets of peaks in NaAc solutions (pH 6.0), blue line in Fig. 12. Two cathodic peaks between −0.25 and −0.35 V are caused by catalytic proton reduction through the amine group, eqn (2) where the two cysteamine conformations in the monolayer cause two peaks for the same reaction.[74] A second pair of peaks around −0.65 V is due to reductive desorption and re-adsorption of the SAMs, eqn (3).

$$\mathrm{Au–S–CH_2–CH_2–NH_3^+ + e^- \rightarrow Au–S–CH_2–CH_2–NH_2 + \tfrac{1}{2}H_2} \quad (2)$$

$$\mathrm{Au–S–CH_2–CH_2–NH_3^+ + e^- \rightarrow Au + {}^-S–CH_2–CH_2–NH_3^+} \quad (3)$$

A highly ordered cysteamine monolayer is observed in the potential range of −0.15 to + 0.2 V, while oxidation of cysteamine begins at positive potentials above 0.3 V and the smooth surface covered by well organized molecules is replaced by short "worm-like" structures, Fig. 12A. Such a feature is more clearly visible at the potential −0.28 V, corresponding to the cathodic peaks of proton reduction catalyzed by the amine group, Fig. 12B. The size and width of "the worms" remain the same as previously. However, the worm-like structures become shorter but wider when the substrate potential approaches −0.62 V or more negative potentials, which is close to the peak potential for reductive desorption of the cysteamine monolayer, Fig. 12C. Significant changes appear at a potential slightly more negative than −0.62 V, Fig. 12D and E. These "worm-like" structures extend to 2-dimensional islands, suggesting that the atoms on the Au(111) surface are dynamically rearranged. When the potential is shifted further negatively to the dihydrogen evolution region, the islands expand and combine with each other, giving a flat surface again, Fig. 12F–H. Note that the herringbone structures do not reappear, meaning that reconstruction lines cannot regenerate even at a very negative

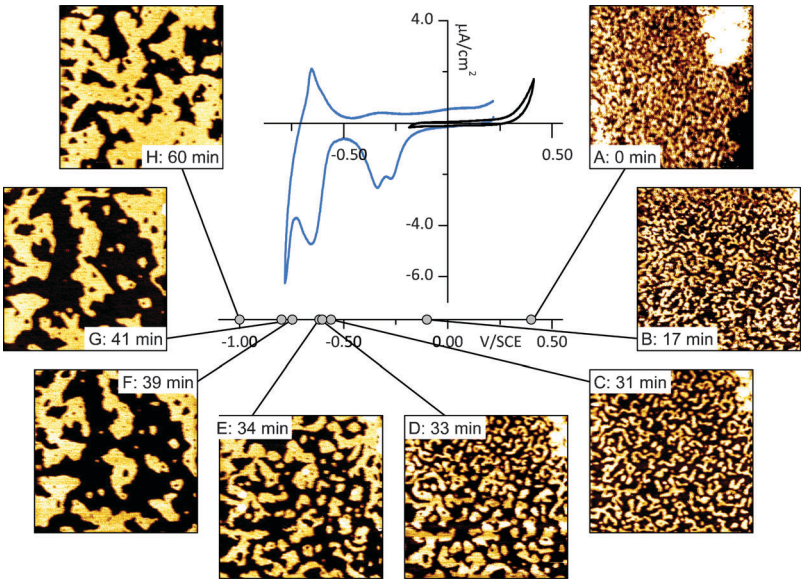

Fig. 12 *In situ* STM observations of potential-dependent structural transforming dynamics of a cysteamine monolayer on Au(111) surfaces. The images were recorded in 5 mM NaAc buffer (pH 6.0) under Ar protection. Working potentials were: (A) 0.36 V, (B) −0.28 V, (C) −0.62 V, (D) and (E) −0.65 V, (F) −0.78 V, (G) −0.85 V and (H) −1.0 V *vs.* SCE.

potential −1.0 V, Fig. 12H. The total coverage of the flat areas at −1.0 V (Fig. 12H) is larger than that at −0.85 V (Fig. G) or −0.75 V (Fig. H). This is caused by deposition of gold from the dissociated Au-cysteamine, which desorbs into the solution due to reductive desorption at negative potentials. This observation is in contrast to SAMs of alkanethiols in basic solution, in which reconstruction lines were observed after the SAMs were reductively desorbed.[106] The *in situ* STM study has thus presented a highly dynamic cysteamine SAM that also depends notably on the potential of the substrate.

In spite of the absence of a redox group in homocysteine, the voltammetry of homocysteine monolayers gives a pair of well-defined sharp peaks at −0.06 V *vs.* SCE in pH 7.7, Fig. 13. Both peak midpoint potential and height depend on solution pH.[75] The peak potentials are shifted negatively at a high pH, while the peak heights decay at either high or low pH and reach a maximum at pH 7.7. The peak half-width also depends on the scan rate and gives a value of 24 mV at a scan rate of 5 mV s^{-1}. This value is significantly smaller than 90 mV, the value for an ideal diffusionless electrochemical redox reaction. The origin of these peaks is still a puzzle, but a speculation offered and strongly supported by *in situ* STM, is that the origin of the peak is capacitive and caused by structural reorganization of the homocysteine molecules in a narrow potential range around the potential of zero charge.[75]

A study of the homocysteine monolayer *dynamics* at various potentials by *in situ* STM is illustrated in Fig. 13. A frizzy layer with small black holes is found at −0.31 V, Fig. 13A, while small domains with highly ordered homocysteine molecules become visible at −0.18 V, Fig. 13B. The coverage of the ordered domains reaches a maximum at −0.07 V, *i.e.* very close to the midpoint potential of the peak, −0.06 V in Fig. 13 C, and has decreased at 0.02 V, Fig. 13D. A more disordered adlayer appears at 0.18 V, Fig. 13E. This observation suggests that homocysteine molecules pack in a lattice only around the peak potential. In fact, high-resolution images of homocysteine presented in Fig. 8D were obtained only around the peak potential. The whole process is reversible and reproducible with respect to the potential scans. A mechanism for monolayers of ordered/disordered switching is shown in Fig. 13F, in which $–COO^-$ and $–NH_3^+$ from homocysteine at neutral pH can approach the Au(111) surface around the fixed anchor Au–S during the potential sweep, at the potentials positive or negative of the peak potential, respectively. Flexibility of the –C–C– unit gives smooth flipping under the driving force of the electric field caused by the applied potential. The evidence from *in situ* STM thus offers a plausible explanation for the origin of the non Faradaic, apparently highly cooperative voltammetric peaks of the homocysteine monolayer.[75]

5. Theoretical computations and STM image simulations

Multifarious patterns of widely differently functionalized alkanethiol SAMs have been mapped to single-molecule and sub-molecular resolution by *in situ* STM directly in aqueous electrolyte solution. Structural mapping has been strongly supported by electrochemical studies of the reductive desorption process in particular, based on the same SAMs and on the same single-crystal, atomically planar electrode surfaces. *In situ* STM is, however, fundamentally rooted in electronic *conductivity* and the quantum mechanical tunnelling effect, rather than solely in topography. Theoretical and large-scale computational support is therefore needed in detailed image interpretation and understanding of all the many facets of the alkanethiol-based SAM packing and *in situ* STM contrast features.[133]

The variety of straight *versus* singly and doubly branched, otherwise non-functionalized alkanethiols constitutes one system class where computational support has been decisive

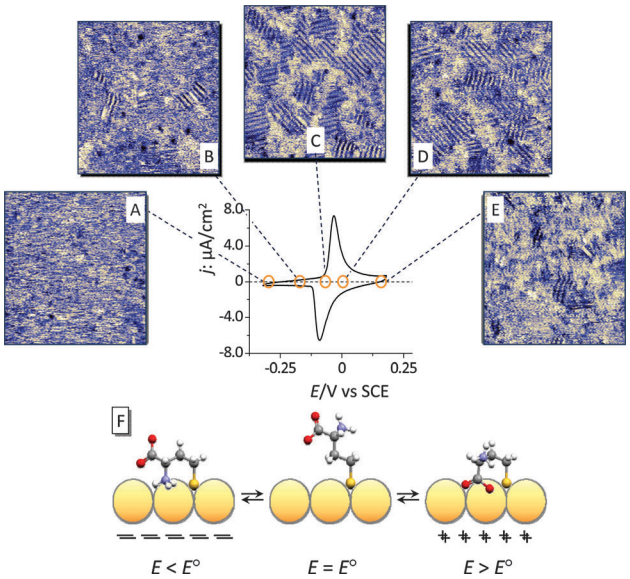

Fig. 13 Potential dependent STM images of homocysteine[75] on Au(111) in 5 mM PB (pH = 7.7). I_t = 0.10 nA, V_{bias} = −0.10 V, oxygen-free environment. Working potential (A) −0.31 V, (B) −0.18 V, (C) −0.07 V, (D) 0.02 V and (E) 0.18 V *vs.* SCE. Scan area: 50 × 50 nm^2. Dotted lines show the working electrode potential, where images were obtained. (F) A model of three-state phenomenological structural frame, Left: Negative potentials, Hcy in a bent conformation with the $-NH_3^+$ group contacting the electrode surface. Middle: Potentials close to neutral surface charge, Hcy in a stretched conformation, giving laterally ordered surface domains, with the $-COO^-$ group parallel to the surface. Right: Positive potentials, Hcy again in a bent configuration now with the $-COO^-$ group adjacent to the Au(111)-surface.

in the clarification of the highly subtle interplay between Au–S binding sites (hollow sites, bridge, and a-top sites, or intermediates in between), composite lateral interactions, and Au-atom "mining" out of the planar Au-electrode surfaces.[124,126,134,135] The latter energetic expenditure is compensated by more favourable Au–S bonding energetics to the now "loosened" but still surface-bound Au-atoms.

A second class of, functionalized alkanethiol SAMs where large-scale theoretical and computational efforts have disclosed new insights to the strongly solvated L-cysteine[129] and cysteamine[74] SAMs. Solvation effects have been included in complementary ways. Both strong and illuminating continuum models and large-scale molecular dynamics based views have been combined with quantum chemical computations at the density functional level, adding immensely to the common understanding of the molecular packing in these functionalized alkanethiol SAMs and of the corresponding *in situ* STM contrasts.

The DFT computations of *in situ* STM L-cysteine on Au(111)-surface models in a dielectric solvent directly pertaining to the commonly applied constant current mode and with electronic coupling to a model tungsten tip rather than less-specific electronic charge density have been one computational approach.[129] Image contrasts could be reproduced but maximum electrostatic stability of clusters of exactly *six* zwitterionic cysteine molecules in a continuous dielectric medium was also found. This particular configuration follows closely the pattern observed when ammonium acetate, pH 4.6 is the electrolyte medium and Au(111) the substrate surface, although other packing modes in different electrolytes have also been reported. This kind of computational support applies no less strikingly in the sub-molecular image interpretation of *in situ* STM of L-cysteine on a Au(110)-electrode surface where the three submolecular lobe features could be assigned to the three functional groups of the molecules: the Au–S bond, the ammonium group, and the carboxylate group.[118]

Even more detailed insight into the complex interplay between covalent and non-covalent adsorption forces on the one hand and solvation forces on the other hand is offered by the cysteamine case with the electrostatically positively charged ammonium terminal group on Au(111)-electrode surfaces in aqueous buffer under electrochemical potential control. As noted, the dual *in situ* STM contrasts in the ($\sqrt{3}$ × 4)R30° lattice emerge after real-time movie recording with anaerobic atmosphere as an absolute pre-requisite for high-resolution imaging. Each of the two contrasts represents a single molecule as framed by coverage determination based on voltammetric reductive desorption. The dual contrasts were paralleled by two other, closely spaced voltammetric peaks assigned to catalytic dihydrogen evolution *via* the two differently configured cysteamines.

A comprehensive combined molecular dynamics and DFT study could notably offer a detailed rationale for *all* the data.[74] The two *in situ* STM contrasts could, first clearly be associated with two different cysteamine surface orientations with different tilt angles. This packing mode was, secondly controlled by all the Au–S and intermolecular interactions as well as solvation forces where the strength of the latter was competitive with the Au–S forces or even prevailed over the latter. Thirdly, the specific *in situ* STM contrasts with all the strong solvation forcers included could be assigned to specific cysteamine fragments or pure adsorbed solvent (water) molecules. The strongest contrast in the dual *in situ* STM contrasts reflected the molecular fragment closest to the *in situ* STM tip, *i.e.* the ammonium functional group but, notably with substantial electronic density and *in situ* STM contrast contribution from the Au–S covalent unit transmitted through the molecular cysteamine adsorbate. In other words, substantial *in situ* STM tunnelling contributions appeared to be spatially shifted due to the through-bond conduction mechanisms. In crucial ways the Au(111)/cysteamine/aqueous electrolyte system therefore illustrates the challenges regarding single-molecule *in situ* STM imaging posed by the otherwise apparently well known pure and chemically functionalized alkanethiol SAMs. Comprehensive studies of this system, however, also shows how the challenges can be met by the combined efforts of state-of-the-art single-molecule experimental electrochemical science combined with adequate computational support.

6. Some examples of applications of SAMs

The high stability of alkanethiol-based SAMs crucially rooted in the strong chemical Au–S bonding has ensured a wide range of applications in physics, chemistry, biochemistry, materials

science and engineering, and nanotechnology. In this section, we discuss several examples of SAM applications.

6.1 SAMs used to immobilize metalloproteins

Protein monolayers with biological function retained are crucial for studying interfacial electron transfer of metalloproteins as well as for applications for example in biosensors. A molecule with a thiol at one end and another functional group in the opposite end can form SAMs on a gold substrate providing tailor-made surfaces, in which the functional group can bind to amino acid residues on the metalloprotein surface through electrostatic interaction, hydrogen bonding, or hydrophobic forces.[136] The SAM serves not only as a linker to connect protein molecules but also as an electronic wire for promoting electron transport. A number of protein monolayers including the blue copper protein azurin,[95,96] the heme protein cytochrome c_4,[91] the iron–sulfur protein ferredoxin,[69] and the blue copper enzyme nitrite reductase (NiR)[137] have been successfully addressed and mapped to single-molecule resolution by employing this strategy together with the combination of single-crystal electrochemistry and *in situ* STM. Immobilization of proteins on SAMs ensures well-controlled orientation of the protein, fast electron transfer and high efficiency due to the very small amount of protein used. So far there is, however, no general rule to guide the choice of a specific thiol for a given protein. For example, alkanethiols with methyl end group appear as ideal linkers for azurin,[95] but they are not suitable for the blue copper enzyme nitrite reductase. Cysteamine with a $-NH_2$ end group is here instead found to be efficient molecule for attachment of NiR on Au(111)-electrode surfaces.[137] Comprehensive laboratory work is generally required to screen thiols with different functional groups for each individual protein.

6.2 SAMs used to fabricate chemical and biochemical sensors

SAMs offer an opportunity for fabrication of chemical sensors.[138] The functional group in the SAM would interact selectively with the targeted molecules or ions. For example, cysteine molecules in SAMs bind Cu^{2+} in aqueous solution with a 2 : 1 ratio of cysteine to bound Cu^{2+}. Electrochemical sensors for Cu^{2+} in environmental samples were constructed by cysteine SAMs on Au electrodes with a detection limit down to 5 ppm.[139] In a similar strategy, thiol containing polymers with functional groups can be used for construction of various sorts of sensors. As an example, the thiophene derivative, (4-benzeno-15-crown-5 ether)thiophene-3-methyleneamine (BTA) was electropolymerized on a gold surface to form densely packed nanoparticle adlayers, with selective sensitivity to K^+ with a linear dependence of the ion concentration over 4 orders of magnitude.[140]

Much effort has been devoted to the development of biosensors over the last 20 years.[141] High sensitivity, small size, rapid response and good biocompatibility are highly desired for modern biosensors. SAMs have been used as an essential component for coupling a biological element such as an enzyme with a transducer such as an electrode. Pioneering work was initiated by Willner's group in the early 1990s by using chemical coupling of surface-bound cysteamine to proteins and enzymes for specific biological metabolite targeting.[142,143] For example, the cysteamine SAMs provide an amine terminated surface which can react chemically with *trans*-stilbene-(4,4′-diisothiocyanate)-2,2′-disulfonic acid (DIDS) and form a covalent bond. DIDS is a symmetrical bifunctional reagent, one end of which reacts with cysteamine and the other end with amino groups in the proteins.[144] In this way, monolayers of glutathione reductase, glucose oxidase, glucose dehydrogenase, acetylcholine esterase and choline oxidase have been constructed.[145] Certain SAMs and their applications in larger molecular architectures to design and construct biosensors have been reviewed several times recently.[146,147]

6.3 SAMs used to stabilize metallic nanostructures and to construct functional bioinorganic hybrids

Preparation of metallic nanostructures including nanoparticles and nanorods or nanowires is one of core activities in nanoscience and nanotechnology. For example, synthetic chemistry can offer feasible ways to produce gold nanoparticles (AuNPs) with well controlled size and shape in a large scale.[148] Naked AuNPs are unstable in solution, but aggregation can be prevented by a suitable coating layer around the nanoparticles. SAMs of thiols with different functional end groups and various lengths have been used as powerful ligands to stabilize the freshly formed AuNPs.[148] The –SH is anchored on the AuNP surface, while the functional end group faces the solution. The functional end groups can be further used as linkers for attachment of a metalloprotein.[149,150]

As an example, the AuNP-cyt *c* hybrids with 3.5 nm AuNPs have been constructed using a thiol with a $-COO^-$ end group, where $-COO^-$ binds to the positively charged pocket around the heme centre in cytochrome *c* (cyt *c*) by electrostatic interaction.[149] The hybrid contains the protein and gold nanoparticles in a stoiciometric 1 : 1 ratio, and possesses properties from both components. The hybrids could further be immobilized on Au(111)-electrode surface *via* a cysteamine SAM, the amine end group of which binds to the carboxylate-based coating layer of the AuNP. An order of magnitude faster interfacial electron transfer was achieved when cyt *c* was part of an AuNP-cyt *c* hybrid monolayer than a cyt *c* monolayer alone under similar experimental conditions. The AuNPs therefore play a key role in the enhancement of the electron transfer rate of cyt *c*. More sophisticated bioinorganic hybrids with various functional components can be designed and constructed by using SAMs in similar ways.

6.4 SAMs used for single-molecule electronics

Driven by the development of molecular electronic devices in nanotechnology, demand has increased for the highly challenging measurement and understanding of charge transport in a single molecule. Individual molecular electronic behaviour can now be experimentally addressed using several strategies, some of which have been reviewed elsewhere. As an example, in one core strategy based on STM technique,[151,152] a gold tip is employed for molecular conductivity measurements. Targeted systems are these molecules containing two –SH groups, one at each of the two ends of the molecule.[153] The

molecule is adsorbed on the gold surface by one –SH group, while the other –SH group attaches to the STM gold tip when the tip is scanned over the monolayer. A single molecular wire between the gold tip and gold substrate is formed in this way. Tunnelling spectroscopy for example, current (I)–voltage (V), current(I)–distance (s) or current (I)–time (t) curves can be directly recorded.[153–160] A number of molecules that involve both redox and non-redox molecules such as viologen α, ω-dithiols,[153] alkanedithiols,[154] conjugated molecular bridges,[156] pyrrolo-tetrathiafulvalene,[157] have been investigated in detail. Systematic analysis of the results shows that the molecular conductivity depends on the molecular structure, conformation,[158,160] solvation,[159] temperature,[154] and redox properties,[157] *etc*. Comprehensive theoretical efforts at different levels to support the understanding of the widely different single-molecule conductivity mechanisms of redox and non-redox molecules have become available.[154] Single-molecule conductivity is now a major interdisciplinary research field. Thiol-based SAMs remain, however a crucial building block to ensure optimal molecular surface binding and local environment. The new single-molecule areas offer together clues towards the realization of forthcoming new generation molecular electronic devices.

7. Comments and perspectives

In addition to these applications summarized in Section 6.3, other real or putative areas for future thiol-based SAM research and development are becoming visible. A few areas can be noted:

We have repeatedly encountered cysteine as a natural amino acid with a free –SH group, that forms attractive and surface specific SAMs on gold surfaces which have emerged as primary targets for comprehensive experimental and theoretical *in situ* STM efforts. Assembling of peptides and proteins through cysteine offers a biological aspect.[161] Protein engineering can introduce in principle any specific amino acids in a target protein and offers routes to a wealth of functional protein monolayers on metallic surfaces. Previous and recent efforts based on yeast cyt c[162] and human insulin[163] have testified to the value of this potentially powerful approach.

Systematic investigations of SAMs on other metal or semiconductor substrates, for example by formation of S-Me or N–Me bonds would extend the applications particularly in heterogeneous catalysis and perhaps molecular electronics. Besides S–Au, S–Ag, S–Pt and N–Pt are other chemical bonds, which can serve as a basis for new types of electrochemically controlled monolayer formation.

Most SAMs discussed in this communication refer to *in situ* STM and target studies in aqueous media. *In situ* STM can, however, be extended to other environments such as ionic liquids[113,164–168] and organic solvents. These alternative environments can offer, for example much wider working potential windows as well as a wealth of thiols with all sorts of functional groups. An obstacle arises in the form of the tip coating materials. Well-developed tip coating materials for aqueous solution such as nail polish[82] or Apiezon wax[83] do not withstand organic solvents. This obstacle can, however, perhaps be classified as a ''technicality'', and suitable other tip coating materials such as polyethylene are well on the road to being tested and generally introduced.

As any advanced techniques, there are great advantages offered by *in situ* STM but also some limitations. The former have been reviewed in the discussion above. One limitation noted is the need for heavy theoretical and computational support in, for example, image interpretation but we have also seen that this can be turned to the better in the form of amazing detail once the challenging computations have been undertaken. A ''philosophical'' concern that remains is, however, that spurious STM and *in situ* STM signals, *i.e*. from ''background'', the solution, local substrate surface structures or from somewhere else, *i.e*. artifacts keep ''cropping up''. Improving the sample quality and the purity of solution and supporting electrolyte is one way to avoid possible artifacts. In addition, reference experiments and highly controlled experiments should be warranted. Representative data should, further, be statistically high on both reproducibility and stability. Finally, complementary surface-related methods, such as Raman spectroscopy, fluorescence spectroscopy, X-ray photo electron spectroscopy (XPS) and other surface spectroscopies are essential in the quest for further advancement in characterization and understanding of the exciting surface molecular chemical structure and dynamics which is now being brought within reach.

8. Concluding summary

Self-assembled molecular monolayers of thiol-based organic molecules have come to represent an impressive variety of controlled surface structures at the same time immensely rich in structural detail that have reached not only the single-molecule but even the sub-molecular level. Thiol-based SAM structures can be based on hydrophobic and hydrophilic, electrostatically neutral or positively and negatively charged or both, structurally small or voluminous end groups, and materially rigid or soft two-dimensional properties. In some cases such as straight-chain alkanethiol surface packing modes vary little as the chain length increases but as soon as functional end groups or structural branching are introduced highly diverse packing almost close to being specific to the individual molecular structure arises. Some packing lattices are relatively simple such as straight-chain alkanethiol lattices, but multifarious other modes arise such as for the branched alkanethiols.

In the widest sense, the alkanethiol-based SAMs offer unique options for addressing many aspects of the physics and chemistry of molecular surface binding. Differences between UHV environment and the chemically more realistic *in situ* aqueous and other condensed matter environment have for example been addressed. While tunnelling conduction mechanisms of non-redox molecules such as the organic thiols may not differ strongly, the two-dimensional packing and other surface structural features are drastically different for hydrophilic or electrostatically charged thiol-based SAMs. Solvation forces are fully competitive with the Au–S binding forces themselves in the packing control for these molecules such as strikingly illuminated by L-cysteine and cysteamine. Different Au-substrate atomic structures such as the different

low-index Au(111)-, Au(100)- and Au(110)-surfaces offer other highly different varieties of surface packing modes.

The alkanethiol-based SAMs have also offered unique targets for large-scale computational efforts. Objectives extend all the way from structural properties, energetics, charge population of adsorbate molecular orbitals, packing and Au–S binding modes, and the effects of the Au-substrate atomic structures to direct tunnelling current mechanisms and (*in situ*) STM imaging under realistic *in situ* working conditions. The dynamics of the *in situ* SAM formation process in real time and at the single-molecule level has been followed as illustrated by the 1-propanethiol case. The amino acid L-cysteine has turned out as a striking core target molecule that now offers prospects for the understanding of all these crucial SAM issues at the molecular and sub-molecular levels of resolution. As a result of efforts of many groups, the surface chemistry and physics of alkanethiol-based SAMs on well-defined Au-surfaces in both UHV and aqueous electrolyte solution are now better understood than for any other molecular SAM systems.

With the surface structure and dynamics increasingly well understood, other options for exploiting the atomically well understood thiol-controlled molecular binding and SAM structures in new challenging areas come to mind. Redox metalloproteins such as yeast cytochrome *c* (*Saccharomyces cerevisiae*), human and other mammalian insulin forms or the blue copper protein azurin (*Pseudomonas aeruginosa*) contain exposed thiol or disulfide groups. The latter are highly likely to break and establish individual Au–S contacts on adsorption on well-defined single-crystal Au-surfaces. These proteins have offered a wealth of novel insights in pure and applied protein/Au-surface science very much rooted in fundamental *in situ* thiol-based surface science. Molecular scale thiol-based surface science has, further come to stand forward in the understanding of the single-molecule behaviour of "smart" molecules linked to enclosing Au-electrodes *via* Au–S bond formation in condensed matter environment. "Rectification", "amplification", and other "smart" electronic functions at the single-molecule level and in chemical condensed matter environment are standing forward with increasing visibility. Strong and well-defined chemical binding of these remarkable molecules to the enclosing (*in situ*) STM and other nanoscale electrodes is a pre-requisite for efficient functionality. The Au–S bond and electrochemical thiol SAMs here provide unique guidance. Transition metal complexes, redox metalloproteins, and thiol-linked DNA-based molecules are all offered as pure and applied single-molecule targets in these wider thiol-based SAM perspectives.

A final novel thiol-based SAM-perspective is to exploit the diversity of well-defined (atomically planar, single-crystal) SAM-modified surfaces as substrates for adsorption and retained function of much more sophisticated redox proteins and other biological macromolecules. Biosensor function and other direct applied thiol SAM-based exploitation was also noted. The electrochemical electron transfer as well as sophisticated enzyme function of redox metalloproteins and metalloenzymes on multifariously thiol-based modified Au(111)-electrode surfaces have testified to the importance of these novel perspectives. In quite recent studies the growth and organization of whole living cells in the form of bacterial biofilms on alkanethiol-modified Au(111)-electrode surfaces have added other new biological insights based on the detailed understanding of pure and functionalized alkanethiol-based SAMs. Structural and dynamic single-molecule mapping, exploitation of the Au-binding of "smart" molecules including redox and non-redox proteins, and well-defined metallic surface padding for further biological protein and biological cell function are other evolving pure and applied perspectives that our fundamental understanding of the single-molecule structure and dynamic behaviour of electrochemical thiol-based SAM can offer.

Acknowledgements

Financial support from the Lundbeck Foundation and the Danish Research Council for Technology and Production Sciences (Contract No. 274-07-0272) is acknowledged.

References

1 A. T. Hubbard, *Chem. Rev.*, 1988, **88**, 633–656.
2 G. A. Somorjai, *Chemistry in Two Dimensions: Surfaces*, Cornell University, Ithaca, NY, 1981.
3 A. T. Hubbard, *CRC Crit. Rev. Anal. Chem.*, 1973, **3**, 201.
4 A. T. Hubbard, J. L. Stickney, M. P. Soriaga, V. K. F. Chia, S. D. Rosaaco, B. C. Schardt, T. Solomun, D. Song, J. H. White and A. Wieckowski, *J. Electroanal. Chem.*, 1984, **168**, 43.
5 F. P. Zamborini and R. M. Crooks, *Langmuir*, 1997, **13**, 122–126.
6 F. T. Arce, M. E. Vela, R. C. Salvarezza and A. J. Arvia, *J. Chem. Phys.*, 1998, **109**, 5703–5709.
7 F. T. Arce, M. E. Vela, R. C. Salvarezza and A. J. Arvia, *Langmuir*, 1998, **14**, 7203–7212.
8 R. Yamada and K. Uosaki, *Langmuir*, 1998, **14**, 855–861.
9 R. G. Nuzzo and D. L. Allara, *J. Am. Chem. Soc.*, 1983, **105**, 4481–4483.
10 A. Ulman, *Chem. Rev.*, 1996, **96**, 1533.
11 F. Schreiber, *Prog. Surf. Sci.*, 2000, **65**, 151–256.
12 G. E. Poirier, *Chem. Rev.*, 1997, **97**, 1117–1127.
13 D. P. Woodruff, *Phys. Chem. Chem. Phys.*, 2010, **12**, 7211–7221.
14 E. Delamarche, B. Michel, H. A. Biebuyck and C. Gerber, *Adv. Mater.*, 1996, **8**, 719–729.
15 A. Badia, R. B. Lennox and L. Reven, *Acc. Chem. Res.*, 2000, **33**, 475–481.
16 A. S. Duwez, *J. Electron Spectrosc. Relat. Phenom.*, 2004, **134**, 97–138.
17 R. K. Smith, P. A. Lewis and P. S. Weiss, *Prog. Surf. Sci.*, 2004, **75**, 1–68.
18 J. C. Love, L. A. Estroff, J. K. Kriebel, R. G. Nuzzo and G. M. Whitesides, *Chem. Rev.*, 2005, **105**, 1103–1169.
19 G. Liu, S. Xu and Y. Qian, *Acc. Chem. Res.*, 2000, **33**, 457–466.
20 T. Kondo and K. Uosaki, *J. Photochem. Photobiol., C*, 2007, **8**, 1–17.
21 S. Lee, J. Park, R. Ragan, S. Kim, Z. Lee, D. K. Lim, D. A. A. Ohlberg and R. S. Williams, *J. Am. Chem. Soc.*, 2006, **128**, 5745–5750.
22 B. Damaskin, O. A. Petrii and V. V. Batrakov, *Adsorption of Organic Compounds on Electrodes*, Plenum Press, New York, 1972.
23 J. Richer and J. Lipkowski, *J. Electrochem. Soc.*, 1986, **133**, 121–128.
24 Z. Shi, J. Lipkowski, M. Gamboa, P. Zelenay and A. Wieckowski, *J. Electroanal. Chem.*, 1994, **366**, 317–326.
25 O. M. Magnussen, *Chem. Rev.*, 2002, **102**, 679–725.
26 T. Wandlowski, Phase transitions in two-dimensional adlayers at electrode surfaces: Thermodynamics, kinetics and structural aspects, in *Encyclopedia of Electrochemistry*, ed. M. Urbakh and M. Gileadi, Wiley-VCH, 2002, vol. 1, pp. 383–467.
27 T. Dretschkow and T. Wandlowski, Structural transitions in organic adlayers – a molecular view, in *Solid-Liquid Interface*

Properties and Processes – A Surface Science Approach, ed. K. Wandelt, *Top. Appl. Phys.*, Springer-Verlag, 2003, vol. 85, pp. 259–321.
28 B. Han, Z. Li, C. Li, I. Pobelov, G. Su, R. Aguilar-Sanchez and T. Wandlowski, *Top. Curr. Chem.*, 2009, **287**, 181–255.
29 F. Cunha and N. J. Tao, *Phys. Rev. Lett.*, 1995, **75**, 2376–2379.
30 F. Cunha, N. J. Tao, X. W. Wang, Q. Jin, B. Duong and J. D'Agnese, *Langmuir*, 1996, **12**, 6410–6418.
31 T. Wandlowski, K. Ataka and D. Mayer, *Langmuir*, 2002, **18**, 4331–4341.
32 T. Sawaguchi, F. Mizutani and I. Taniguchi, *Langmuir*, 1998, **14**, 3565.
33 T. Sawaguchi, F. Mizutani, S. Yoshimoto and I. Taniguchi, *Electrochim. Acta*, 2000, **45**, 2861–2867.
34 Q. Jin, J. A. Rodriguez, C. Z. Li, Y. Darici and N. J. Tao, *Surf. Sci.*, 1999, **425**, 101–111.
35 L. Wan, Y. Hara, H. Noda and M. Osawa, *J. Phys. Chem. B*, 1998, **102**, 5943–5946.
36 T. Baunach, V. Ivanova, D. A. Scherson and D. M. Kolb, *Langmuir*, 2004, **20**, 2797.
37 W. Zhou, T. Baunach, V. Ivanova and D. M. Kolb, *Langmuir*, 2004, **20**, 4590–4595.
38 W. Li, W. Haiss, S. Floate and R. J. Nichols, *Langmuir*, 1999, **15**, 4875–4883.
39 B. Roelfs, E. Bunge, C. Schroter, T. Solomun, H. Meyer, R. J. Nichols and H. Baumgartel, *J. Phys. Chem. B*, 1997, **101**, 754–765.
40 E. Bunge, R. J. Nichols, H. Baumgartel and H. Meyer, *Ber. Bunsenges. Phys. Chem.*, 1995, **99**, 1343–1246.
41 E. Bunge, R. J. Nichols, B. Roelfs, H. Meyer and H. Baumgartel, *Langmuir*, 1996, **12**, 3060–3066.
42 E. Bunge, S. N. Port, B. Roelfs, H. Meyer, H. Baumgartel, D. J. Schiffrin and R. J. Nichols, *Langmuir*, 1997, **13**, 85–90.
43 T. Osaka, T. Sawaguchi, F. Mizutani, T. Yokoshima, M. Takai and Y. Okinaka, *J. Electrochem. Soc.*, 1999, **146**, 3295–3299.
44 G. J. Su, H. M. Zhang, L. J. Wan, C. L. Bai and T. Wandlowski, *J. Phys. Chem. B*, 2004, **108**, 1931–1937.
45 Z. Li and T. Wandlowski, *J. Phys. Chem. C*, 2009, **113**, 7821–7825.
46 B. Han, Z. Li and T. Wandlowski, *Anal. Bioanal. Chem.*, 2007, **388**, 121–129.
47 M. Kunitake, T. Hattori, S. Miyano and K. Itaya, *Langmuir*, 2005, **21**, 9206–9210.
48 M. Kunitake, U. Akiba, N. Batina and K. Itaya, *Langmuir*, 1997, **13**, 1607–1615.
49 N. Batina, M. Kunitake and K. Itaya, *J. Electroanal. Chem.*, 1996, **405**, 245–250.
50 S. Yoshimoto, A. Tada, K. Suto, R. Narita and K. Itaya, *Langmuir*, 2003, **19**, 672–677.
51 S. Yoshimoto, A. Tada and K. Itaya, *J. Phys. Chem. B*, 2004, **108**, 5171–5174.
52 S. Yoshimoto, N. Higa and K. Itaya, *J. Am. Chem. Soc.*, 2004, **126**, 8540–8545.
53 S. Yoshimoto, A. Tada, K. Suto and K. Itaya, *J. Phys. Chem. B*, 2003, **107**, 5836–5843.
54 K. Suto, S. Yoshimoto and K. Itaya, *J. Am. Chem. Soc.*, 2003, **125**, 14976–14977.
55 S. Yoshimoto, R. Narita, E. Tsutsumi, M. Matsumoto, K. Itaya, O. Ito, K. Fujiwara, Y. Murata and K. Komatsu, *Langmuir*, 2002, **18**, 8518–8522.
56 S. Yoshimoto, E. Tsutsumi, R. Narita, Y. Murata, M. Murata, K. Fujiwara, K. Komatsu, O. Ito and K. Itaya, *J. Am. Chem. Soc.*, 2007, **129**, 4366–4376.
57 K. Uosaki, S. Ye, H. Naohara, Y. Oda, T. Haba and T. Kondo, *J. Phys. Chem. B*, 1997, **101**, 7566.
58 Y. Nagahara, M. Hara, S. Yoshimoto, J. Inukai, S. Yau and K. Itaya, *J. Phys. Chem. B*, 2004, **108**, 3224–3230.
59 H. F. Waibel, M. Kleinert, L. A. Kibler and D. M. Kolb, *Electrochim. Acta*, 2002, **47**, 1461–1467.
60 L. A. Kibler, M. Kleinert and D. M. Kolb, *Surf. Sci.*, 2000, **461**, 155.
61 H. Naohara, S. Ye and K. Uosaki, *J. Electroanal. Chem.*, 1999, **473**, 2.
62 R. Yamada and K. Uosaki, *J. Phys. Chem. B*, 2000, **104**, 6021–6027.
63 H. Hagenstrom, M. A. Schneeweiss and D. M. Kolb, *Langmuir*, 1999, **15**, 2435–2443.
64 M. J. Esplandiu, H. Hagenstrom and D. M. Kolb, *Langmuir*, 2001, **17**, 828–838.
65 T. Baunach and D. M. Kolb, *Anal. Bioanal. Chem.*, 2002, **373**, 743–748.
66 J. U. Nielsen, M. J. Esplandiu and D. M. Kolb, *Langmuir*, 2001, **17**, 3454.
67 M. J. Giz, B. Duong and N. J. Tao, *J. Electroanal. Chem.*, 1999, **465**, 72–79.
68 M. Petri, D. M. Kolb, U. Memmert and H. Meyer, *Electrochim. Acta*, 2003, **49**, 175–182.
69 J. Zhang, H. E. M. Christensen, B. L. Ooi and J. Ulstrup, *Langmuir*, 2004, **20**, 10200–10207.
70 J. Zhang, Q. Chi and J. Ulstrup, *Langmuir*, 2006, **22**, 6203–6213.
71 M. Schweizer, M. Manolova and D. M. Kolb, *Surf. Sci.*, 2008, **602**, 3303–3307.
72 J. Zhang, Q. Chi, J. U. Nielsen, E. P. Friis, J. E. T. Andersen and J. Ulstrup, *Langmuir*, 2000, **16**, 7229–7237.
73 F. Loglio, M. Schweizer and D. M. Kolb, *Langmuir*, 2003, **19**, 830–834.
74 J. Zhang, A. Bilic, J. R. Reimers, N. S. Hush and J. Ulstrup, *J. Phys. Chem. B*, 2005, **109**, 15355–15367.
75 J. Zhang, A. Demetriou, A. C. Welinder, T. Albrecht, R. J. Nichols and J. Ulstrup, *Chem. Phys.*, 2005, **319**, 210–221.
76 Y. Dai, C. Meier, U. Ziener, K. Landfester, C. Taubert and D. M. Kolb, *Langmuir*, 2007, **23**, 11058–11062.
77 R. Sonnenfeld and P. K. Hansma, *Science*, 1986, **232**, 211.
78 K. Itaya and E. Tomita, *Surf. Sci.*, 1988, **201**, L507–L512.
79 J. Wiechers, T. Twomey and D. M. Kolb, *J. Electroanal. Chem.*, 1988, **248**, 451–460.
80 D. M. Kolb, *Prog. Surf. Sci.*, 1996, **51**, 109–173.
81 A. A. Gewirth and B. K. Niece, *Chem. Rev.*, 1997, **97**, 1129–1162.
82 K. Itaya, *Prog. Surf. Sci.*, 1998, **58**, 121–248.
83 D. M. Kolb, *Angew. Chem., Int. Ed.*, 2001, **40**, 1162–1181.
84 A. M. Funtikov, U. Linke, U. Stimming and R. Vogel, *Surf. Sci.*, 1995, **324**, L343–L348.
85 A. M. Funtikov, U. Stimming and R. Vogel, *J. Electroanal. Chem.*, 1997, **428**, 147–153.
86 D. M. Kolb, R. Ullmann and T. Will, *Science*, 1997, **275**, 1097–1099.
87 G. E. Engelmann, J. C. Ziegler and D. M. Kolb, *Surf. Sci.*, 1998, **401**, L420–L424.
88 J. Meier, J. Schiøtz, P. Liu, J. K. Nørskov and U. Stimming, *Chem. Phys. Lett.*, 2004, **390**, 440–444.
89 Q. Chi, J. Zhang, E. P. Friis, J. E. T. Andersen and J. Ulstrup, *Surf. Sci.*, 2000, **463**, L641–L648.
90 J. Zhang and J. Ulstrup, *J. Electroanal. Chem.*, 2007, **599**, 213–220.
91 Q. Chi, J. Zhang, T. Arslan, L. Borg, G. W. Pedersen, H. E. M. Christensen, R. R. Nazmudtinov and Jens. Ulstrup, *J. Phys. Chem. B*, 2010, **114**, 5617–5624.
92 A. J. Bard and L. R. Faulkner, *Electrochemical Methods. Fundamentals and Applications*, John Wiley and Son Inc., 2nd edn, 2001.
93 P. S. Jensen, Q. Chi, F. B. Grumsen, J. M. Abad, A. Horsewell, D. J. Schiffrin and J. Ulstrup, *J. Phys. Chem. C*, 2007, **111**, 6124–6132.
94 Q. Chi, J. Zhang, J. U. Nielsen, E. P. Friis, I. Chorkendorff, G. W. Canters, J. E. T. Andersen and J. Ulstrup, *J. Am. Chem. Soc.*, 2000, **122**, 4047–4055.
95 Q. Chi, O. Farver and J. Ulstrup, *Proc. Natl. Acad. Sci. U. S. A.*, 2005, **102**, 16203–16208.
96 Q. Chi, J. Zhang, J. E. T. Andersen and J. Ulstrup, *J. Phys. Chem. B*, 2001, **105**, 4669–4679.
97 Q. Chi, J. Zhang, E. P. Friis, J. E. T. Andersen and J. Ulstrup, *Electrochem. Commun.*, 1999, **1**, 91–96.
98 C. Zhong and M. D. Porter, *J. Am. Chem. Soc.*, 1994, **116**, 11616–11617.
99 M. M. Walczak, C. A. Alves, B. D. Lamp and M. D. Porter, *J. Electroanal. Chem.*, 1995, **396**, 103–114.
100 M. M. Walczak, D. D. Popenoe, R. S. Deinhammer, B. D. Lamp, C. Chung and M. D. Porter, *Langmuir*, 1991, **7**, 2687–2693.
101 D. Hobara, M. Ota, S. Imabayashi, K. Niki and T. Kakiuchi, *J. Electroanal. Chem.*, 1998, **444**, 113–119.

102 M. Nishizawa, T. Sunagawa and H. Yoneyama, *J. Electroanal. Chem.*, 1997, **436**, 213–218.
103 S. Imabayashi, M. Iida, D. Hobara, Z. Q. Feng, K. Niki and T. Kakiuchi, *J. Electroanal. Chem.*, 1997, **428**, 33–38.
104 D. Hobara, K. Miyake, S. Imabayashi, K. Niki and T. Kakiuchi, *Langmuir*, 1998, **14**, 3590–3596.
105 D. Yang, H. Al-Maznai and M. Morin, *J. Phys. Chem. B*, 1997, **101**, 1158–1166.
106 H. Wano and K. Uosaki, *Langmuir*, 2001, **17**, 8224–8228.
107 G. E. Poirier and E. D. Pylant, *Science*, 1996, **272**, 1145–1148.
108 R. Staub, M. Toerker, T. Fritz, T. Schmitz-Hubsch, F. Sellam and K. Leo, *Langmuir*, 1998, **14**, 6693–6698.
109 G. E. Poirier, *Langmuir*, 1997, **13**, 2019–2026.
110 G. E. Poirier, W. P. Fitts and J. M. White, *Langmuir*, 2001, **17**, 1176–1183.
111 G. E. Poirier, *Langmuir*, 1999, **15**, 1167–1175.
112 R. Yamada and K. Uosaki, *Langmuir*, 1998, **14**, 855–861; (*in situ* STM in heptane, time dependence SAM process of alkanethiols on Au(111)).
113 F. Endres, W. Freyland and B. Gilbert, *Ber. Bunsenges. Phys. Chem.*, 1997, **101**, 1075.
114 C. Engelbrekt, K. H. Sørensen, J. Zhang, A. C. Welinder, P. S. Jensen and J. Ulstrup, *J. Mater. Chem.*, 2009, **19**, 7839–7847.
115 A. T. Hubbard, *The Handbook of Surface Imaging and Visualization*, CRC Press, Inc, 1995.
116 D. M. Kolb, *Surf. Sci.*, 2002, **500**, 722–740.
117 J. K. Gimzewski, S. Modesti and R. R. Schlittler, *Phys. Rev. Lett.*, 1994, **72**, 1036–1039.
118 J. Zhang, Q. Chi, R. R. Nazmudtinov, T. Zinkicheva and I. Manyurov, *Langmuir*, 2009, **25**, 2232–2240.
119 O. M. Magussen, J. Wiechers and R. J. Behm, *Surf. Sci.*, 1993, **289**, 139–151.
120 G. J. Su, R. A. Sanchez, Z. Li, I. Pobelov, M. Homberger, U. Simon and T. Wandlowski, *ChemPhysChem*, 2007, **8**, 1037–1048.
121 R. Yamada, H. Wano and K. Uosaki, *Langmuir*, 2000, **16**, 5523–5525.
122 J. Noh, H. S. Kato, M. Kawai and M. Hara, *J. Phys. Chem. B*, 2006, **110**, 2793–2797.
123 H. Kang, N. S. Lee, E. Ito, M. Hara and J. Noh, *Langmuir*, 2010, **26**, 2983–2985.
124 Y. Wang, Q. Chi, N. S. Hush, J. R. Reimers, J. Zhang and J. Ulstrup, *J. Phys. Chem. C*, 2009, **113**, 19601.
125 Q. Chi, J. Zhang and J. Ulstrup, *J. Phys. Chem. B*, 2006, **110**, 1102–1106.
126 Y. Wang, N. S. Hush and J. R. Reimers, *J. Phys. Chem. C*, 2007, **111**, 10878–10885.
127 A. S. Dakkouri, D. M. Kolb, R. Edelstein-Shima and D. Mandler, *Langmuir*, 1996, **12**, 2849–2852.
128 Q. Xu, L. Wan, C. Wang, C. Bai, Z. Wang and T. Nozawa, *Langmuir*, 2001, **17**, 6203–6206.
129 R. R. Nazmudtinov, J. Zhang, T. T. Zinkicheva, I. R. Manyurov and J. Ulstrup, *Langmuir*, 2006, **22**, 7556–7567.
130 A. Kuhnle, T. R. Linderoth, M. Schunack and F. Besenbacher, *Langmuir*, 2006, **22**, 2156–2160.
131 A. Kuhnle, T. R. Linderoth and F. Besenbacher, *J. Am. Chem. Soc.*, 2003, **125**, 14680–14681.
132 A. Kuhnle, T. R. Linderoth, B. Hammer and F. Besenbacher, *Nature*, 2002, **415**, 891–893.
133 M. Sprik, E. Delamarche, B. Michel, U. Rothlisberger, M. L. Klein, H. Wolf and H. Ringsdorf, *Langmuir*, 1994, **10**, 4116–4130.
134 Y. Wang, N. S. Hush and J. R. Reimers, *J. Am. Chem. Soc.*, 2007, **129**, 14532–14533.
135 A. Bilic, J. R. Reimers and N. S. Hush, *J. Chem. Phys.*, 2005, **122**, 094708.
136 J. Zhang, Q. Chi, A. M. Kuznetsov, A. G. Hansen, H. Wackerbarth, H. E. M. Christensen, J. E. T. Andersen and J. Ulstrup, *J. Phys. Chem. B*, 2002, **106**, 1131–1152.
137 J. Zhang, A. C. Welinder, A. G. Hansen, H. E. M. Christensen and J. Ulstrup, *J. Phys. Chem. B*, 2003, **107**, 12480–12484.
138 I. Rubinstein, S. Steinberg, Y. Tor, A. Shanzer and J. Sagiv, *Nature*, 1988, **332**, 426.
139 W. Yang, J. J. Gooding and D. B. Hibbert, *J. Electroanal. Chem.*, 2001, **516**, 10–16.
140 P. Shi, Q. Chi, Z. Li, J. Ulstrup, P. J. Møller and J. Mortensen, *J. Am. Chem. Soc.*, 2007, **129**, 3888–3896.
141 J. J. Gooding and D. B. Hibbert, *TrAC, Trends Anal. Chem.*, 1999, **18**, 525–533.
142 I. Willner, A. Riklim, B. Shoham, D. Rivenzon and E. Katz, *Adv. Mater.*, 1993, **5**, 912.
143 A. Riklin and I. Willner, *Anal. Chem.*, 1995, **67**, 4118.
144 I. Willner and E. Katz, *Angew. Chem., Int. Ed.*, 2000, **39**, 1180–1218.
145 B. Willner, E. Katz and I. Willner, *Curr. Opin. Biotechnol.*, 2006, **17**, 589–596.
146 J. J. Gooding, F. Mearns, W. Yang and J. Liu, *Electroanalysis*, 2003, **15**, 81–96.
147 J. J. Gooding and W. Yang, *Act. Chim.*, 2008, **320–321**, 85–89.
148 C. Daniel and D. Astruc, *Chem. Rev.*, 2004, **104**, 293–346.
149 P. S. Jensen, Q. Chi, F. B. Grumsen, J. M. Abad, A. Horsewell, D. J. Schiffrin and J. Ulstrup, *J. Phys. Chem. C*, 2007, **111**, 6124–6132.
150 P. S. Jensen, Q. Chi, J. Zhang and J. Ulstrup, *J. Phys. Chem. B*, 2009, **113**, 13993–14000.
151 A. Yazdani, D. M. Eigler and N. D. Lang, *Science*, 1996, **272**, 1921.
152 B. Q. Xu and N. J. Tao, *Science*, 2003, **301**, 1221.
153 W. Haiss, H. Zalinge, H. Höbenreich, D. Bethell, D. J. Schiffrin, S. J. Higgins and R. J. Nichols, *Langmuir*, 2004, **20**, 7694–7702.
154 W. Haiss, H. Zalinge, D. Bethell, J. Ulstrup, D. J. Schiffrin and R. J. Nichols, *Faraday Discuss.*, 2006, **131**, 253–264.
155 G. J. Su, R. Aguilar-Sanchez, Z. Li, I. Pobelov, M. Homberger, U. Simon and T. Wandlowski, *ChemPhysChem*, 2007, **8**, 1037–1048.
156 W. Haiss, C. Wang, R. Jitchati, I. Grace, S. Martin, A. Batsanov, S. J. Higgins, M. R. Bryce, C. J. Lambert, P. S. Jensen and R. J. Nichols, *J. Phys.: Condens. Matter*, 2008, **20**, 374119.
157 E. Leary, S. J. Higgins, H. Zalinge, W. Haiss, R. J. Nichols, S. Nygaard, J. O. Jeppesen and J. Ulstrup, *J. Am. Chem. Soc.*, 2008, **130**, 12204–12205.
158 C. Li, I. Pobelov, T. Wandlowski, A. Bagrets, A. Arnold and F. Evers, *J. Am. Chem. Soc.*, 2008, **130**, 318–326.
159 E. Leary, H. Höbenreich, S. J. Higgins, H. Zalinge, W. Haiss, R. J. Nichols, C. M. Finch, I. Grace, C. J. Lambert, R. McGrath and J. Smerdon, *Phys. Rev. Lett.*, 2009, **102**, 086801.
160 S. Martin, F. Giustiniano, W. Haiss, S. J. Higgins, R. J. Whitby and R. J. Nichols, *J. Phys. Chem. C*, 2009, **113**, 18884–18890.
161 H. M. Zhang, Y. Li, X. Xu, T. L. Sun, H. Fuchs and L. F. Chi, *Langmuir*, 2010, **26**, 7343–7348.
162 A. G. Hansen, A. Boisen, J. U. Nielsen, H. Wackerbarth, I. Chorkendorff, J. E. T. Andersen, J. Zhang and J. Ulstrup, *Langmuir*, 2003, **19**, 3419–3427.
163 A. C. Welinder, J. Zhang, D. B. Steensgaard and J. Ulstrup, *Phys. Chem. Chem. Phys.*, 2010, **12**, 9999–10011.
164 F. Endres and W. Freyland, *J. Phys. Chem. B*, 1998, **102**, 10229.
165 L. G. Lin, Y. Wang, J. W. Yan, Y. Z. Yuan, J. Xiang and B. W. Mao, *Electrochem. Commun.*, 2003, **5**, 995–999.
166 L. Lin, J. Yan, Y. Wang, Y. Fu and B. Mao, *J. Exp. Nanosci.*, 2006, **1**, 269–278.
167 Y. Su, Y. Fu, J. Yan, Z. Chen and B. Mao, *Angew. Chem., Int. Ed.*, 2009, **48**, 5148–5151.
168 Y. Fu, Y. Su, D. Wu, J. Yan, Z. Xia and B. Mao, *J. Am. Chem. Soc.*, 2009, **131**, 14728–14737.